Nonlinear dynamic responses of ballasted railway tracks using concrete sleepers incorporated with reinforced fibres and pre-treated crumb rubber

Raj, Anand; Ngamkhanong, Chayut; Prasittisopin, Lapyote; Kaewunruen, Sakdirat

DOI:
10.1515/nleng-2022-0320

Document Version
Publisher's PDF, also known as Version of record

Citation for published version (Harvard):
Raj, A, Ngamkhanong, C, Prasittisopin, L & Kaewunruen, S 2023, 'Nonlinear dynamic responses of ballasted railway tracks using concrete sleepers incorporated with reinforced fibres and pre-treated crumb rubber', *Nonlinear Engineering*, vol. 12, no. 1, 20220320. https://doi.org/10.1515/nleng-2022-0320

Research Article

Anand Raj, Chayut Ngamkhanong*, Lapyote Prasittisopin, and Sakdirat Kaewunruen

Nonlinear dynamic responses of ballasted railway tracks using concrete sleepers incorporated with reinforced fibres and pre-treated crumb rubber

https://doi.org/10.1515/nleng-2022-0320
received June 12, 2023; accepted August 19, 2023

Abstract: Damages on railway sleepers due to heavy impact loads induced by the movement of trains can be reduced by improving their impact resistance. Fibre-reinforced/pre-treated crumb rubber concrete sleepers (RCSs) have the potential to display significant impact resistance to withstand a high-magnitude impact load. The ideal proportions of pre-treated crumb rubber, steel fibres, and polypropylene fibres (PFs) can be identified based on the minimum cost-to-impact energy ratio after conducting a drop weight impact test on prisms. The numerical model developed to assess the behaviour of ballasted tracks has been validated using both simulation results and field measurements. Numerical studies have been conducted on ballasted rail tracks with steel and PF-reinforced/pre-treated RCSs using LS-DYNA software. Dynamic strain rate-dependent material parameters are introduced in the numerical simulations. The nonlinear effect of higher train speeds on dynamic track responses has been highlighted in this article. Although the static load-carrying capacity and modulus of elasticity of rubber concrete are low, their dynamic performance controls the track displacements from exceeding permissible limits. The outcome of this study will provide new insights into the effects of railway concrete sleepers incorporated with reinforced fibres and pre-treated crumb rubber on railway track performance in order to ensure safety and reliability before it is put into services.

Keywords: ballasted railway track, fibre-reinforced concrete, pre-treated crumb rubber, concrete sleeper, dynamic strain rate dependent material model

Nomenclature

A_v	roughness constant
E	modulus of elasticity in Pa
E_d	dynamic modulus of elasticity
E_s	static modulus of elasticity
$\dot{e}$	effective strain rate of concrete under dynamic load
$\dot{e}_{sc}$	effective strain rate of concrete under compressive load
$\dot{e}_{st}$	effective strain rate of concrete under tensile load
f_c	compressive strength in N/mm^2
f_t	flexure strength in N/mm^2
g	acceleration due to gravity (9.81 m/s^2), and h signifies the height of fall in m.
N	number of blows till the appearance of cracks at the bottom of the prism
$S_v(\Omega)$	vertical power spectral density
η_c	enhancement factor for strain rate in compression
η_t	enhancement factor for strain rate in tension
ρ	density in kg/m^3
Ω	spatial frequency of irregularities

*** Corresponding author: Chayut Ngamkhanong,** Department of Civil Engineering, Faculty of Engineering, Chulalongkorn University, Bangkok, Thailand; Advanced Railway Infrastructure, Innovation and Systems Engineering (ARIISE) Research Unit, Chulalongkorn University, Bangkok, Thailand, e-mail: chayut.ng@chula.ac.th
Anand Raj: Department of Civil Engineering, Faculty of Engineering, Chulalongkorn University, Bangkok, Thailand, e-mail: anandrajce@gmail.com
Lapyote Prasittisopin: Department of Architecture, Faculty of Architecture, Chulalongkorn University, Bangkok, Thailand, e-mail: Lapyote.P@chula.ac.th
Sakdirat Kaewunruen: Department of Civil Engineering, School of Engineering, University of Birmingham, Birmingham B15 2TT, United Kingdom, e-mail: s.kaewunruen@bham.ac.uk

Abbreviations

CRH	China Railway High Speed
EMU	Electric Multiple Unit
FRF	frequency response function
I.E	impact energy in Nm
OCS	ordinary concrete sleeper
PFCS	polypropylene fibre-reinforced concrete sleeper
PFRS	polypropylene fibre-reinforced rubber concrete sleeper
RCS	rubber concrete sleeper
SFCS	steel fibre-reinforced concrete sleeper
SFRS	steel fibre-reinforced rubber concrete sleeper

1 Introduction

The railway industry has been successful in moving masses and goods efficiently over land, thereby aiding development in many continents globally [1,2]. Ballasted railway tracks are a widely adopted modern track form catering to various classes of railway operations. Railway sleepers are integral to any ballasted track since they enable load transfer from wagons and maintain track alignments [3–6]. Railway sleepers are generally subjected to both static and dynamic loads. Dynamic loads act on the railway track caused by the movement of train wheels. The magnitude of dynamic loads acting on railway sleepers is classified as the dynamic impact factor, which can vary from small to high attributable to the characteristics of train–track dynamics [7,8]. These dynamic loads become critical in the case of moderate to high-speed trains running over tracks with irregularities [9–11]. Even though significant efforts are put toward the smooth and safe operation of a railway network, sometimes accidents do occur. In moderate-speed and high-speed networks, the fatality of accidents increases manifolds due to the combination of high speed and resultant impact force [12]. The effect of damage caused by an accident on sleepers in such situations can be mitigated by using sleepers with high-impact resistance.

Studies have pointed out that the use of recycled or crumb rubber is a potential method to improve the impact resistance of concrete [13–15]. An increase in the fracture toughness of concrete could increase when aggregates were replaced using crumb rubber particles [16,17]. The energy dissipation capacity of concrete can be improved with the addition of rubber particles [18–22]. The improved damping ratio of rubber concrete makes it suitable for applications to structural vibration mitigation [23,24]. In contrast, the use of rubber particles in concrete was found to adversely affect the compressive strength, flexural strength, and tensile strength of concrete [25–30]. Pre-treatment of rubber particles has been demonstrated as a solution to control the reduction in strength of concrete with recycled rubber. Sodium hydroxide solution and polyvinyl alcohol solution are effective in improving the adhesion between the rubber particles and concrete mix [31,32]. This pre-treatment process has been successfully used in rubber concrete applications.

It has been well established that the addition of steel fibres (SFs) into concrete enhances the impact energy, energy dissipation, and fracture toughness of concrete [33–36]. This trait is brought about by the SFs' ability to bridge the gaps in concrete in the event of the generation of cracks [37–39]. Besides improving the impact resistance of concrete, the addition of SFs in concrete helps to control the reduction of strength characteristics in rubber concrete [40,41]. Alternatively, polypropylene fibres (PFs) can mitigate the effects of shrinkage cracks in concrete [42–45]. They also provide positive results regarding improvement in the impact energy of concrete [46,47]. Using PFs and SFs in combination with rubber particles in concrete has the potential to improve the impact resistance and toughness of concrete as reported by many researchers [40,48–50]. The addition of SFs to rubber concrete can control the stiffness degradation of rubber concrete along with executing crack control [51]. However, it must be noted that in the case of fibre-reinforced concrete, post-peak ductility, and toughness are significantly reduced when subjected to dynamic impact loads [52].

The dynamic characteristics of crumb rubber concrete have been studied to assess its suitability to be used in railway sleepers [53]. It demonstrated that the enhanced damping of crumb rubber concrete can make it ideal for conditions to withstand dynamic impact loads. Parvez and Foster also reported an improvement in the fatigue performance of SF-reinforced concrete sleepers [54]. They also showed that the ability of SFs to bridge the cracks across concrete leads to finer crack width and higher static load-carrying capacity when compared to traditional concrete sleepers. The ability of SFs to control flexural cracks has inspired the development of ultra-high-performance concrete with SFs for non-prestressed concrete sleepers [55]. Though the ultra-high-performance fibre-reinforced concrete sleepers had a greater cross-sectional area when compared to prestressed concrete sleepers, their performance was at par with that of regular prestressed concrete sleepers. The rigid nature of SFs played a vital role in enhancing residual stiffness in sleepers with the addition of SFs as reported by Yoo *et al.* [56]. The reduction in shrinkage cracks and better micro-crack control ability can result in the exploration of the potential of using PFs

in railway sleepers [57]. The enhanced permeability and durability have been portrayed as favourable factors for PF-reinforced concrete to be applied in railway sleepers. Jing *et al.* [58] also studied the loading and cracking pattern of prestressed concrete sleepers with crumb rubber. It was reported that rubber concrete sleepers (RCSs) had lower first-crack loads. Furthermore, Raj *et al.* [59] used steel and PFs in scaled models of rubber concrete railway sleepers and obtained favourable results in terms of the impact resistance of fibre-reinforced RCSs. However, the performance of steel and PF-reinforced rubber concrete sleeper (PFRS) prototypes in actual working conditions is yet to be evaluated. To fill this gap, it is essential to undertake extensive studies to understand the effects of different types of fibre-reinforced RCSs on ballasted railway tracks. Conducting experimental investigations to assess the performance of track components can be economically challenging. In such a scenario, numerical simulations offer a less expensive alternative. Many researchers have effectively applied finite element method to ascertain train–track interaction behaviours by simulating the dynamic effect of train movement on tracks [60–62] utilizing LS-DYNA. Most of the researchers undertaking the numerical simulations of rail track performance have used static modulus of elasticity as their material model [8,63,64]. The nature of the load exerted by the train on the track is rather dynamic. It should also be pointed out that the concrete in sleepers has a modulus of elasticity which gets altered during high-frequency dynamic loads [65]. Hence, it is essential to consider the dynamic material properties of constituent materials while carrying out the simulations. In this study, the effect of dynamic strain rate on the performance of ballasted rail track is explored.

It could thus be pointed out that the extensive damage encountered by concrete sleepers due to their lack of impact resistance could be mitigated only by enhancing their impact resistance. In this context, it was noted that improvement in the energy dissipation capacity and impact resistance of concrete with the addition of crumb rubber has been stated by many researchers [28,66–68]. Therefore, the utilization of steel and PF-reinforced rubber concrete in prestressed concrete railway sleepers has the potential to enhance their impact resistance [59]. As aforementioned, the pre-treatment using polyvinyl alcohol can lead to the adhesion improvement of crumb rubber. Note that the existing studies focus only on laboratory-based small-scale tests. However, the existing research materials fail to establish the suitability of using fibre-reinforced RCSs in the field. Before implementing them in the field, the suitability of utilizing steel and PFRSs must be studied with respect to their performance under the actual operating conditions. Thus, it is essential to examine the behaviour of these sleepers in realistic working scenarios. Numerical simulations help in reducing the cost of actual testing. At the same time, utilizing the dynamic behaviour of materials for numerical simulations with dynamic train loads is also important. Hence, this study focuses on using numerical simulations with a dynamic strain rate model derived from experimental investigations to assess the performance of fibre-reinforced pre-treated RCSs on ballasted railway tracks. The outcome of the research points out to the effectiveness of using fibre-reinforced RCSs in actual practice. This option helps in reducing the amount of precious natural aggregates and reuse dumped tyre rubber on a large scale apart from providing a solution to the lower of impact resistance of existing concrete sleepers.

After establishing the background and relevance of research in Section 1, the material properties and engineering properties of fibre-reinforced concrete are included in Section 2. The details of the numerical investigation are presented in Section 2.1. The free vibration response of sleepers and train track analysis (train vibration, dynamic rail responses, sleeper responses, and ballast responses) are presented in Section 3. Finally, Section 4 presents the main findings of the study.

2 Materials and methods

The reference concrete for the railway sleeper used in the study has a compressive strength of 60 N/mm^2. Ordinary Portland cement, metakaolin, manufactured sand, pre-treated crumb rubber, and crushed stones are used for manufacturing high-strength concrete. The specific gravity of the manufactured sand and crushed stones are 2.67 and 2.79, respectively. Metakaolin (specific gravity: 2.6, pH: 4.5–5.5, and bulk density: 400–500 kg/m^3) is used as supplementary cementing material with weight replacement levels of around 10%. Viscosity-modifying agents and high-range water reducers are also used to improve workability. Rubber herein represents crumb rubber with a pre-treatment process and obtained from tyre retreading centres. It has a specific gravity of 0.65. Care has been taken to match the particle size distribution of crumb rubber and manufactured sand. Figure 1 presents the particle size distribution curves for crumb rubber and manufactured sand. The rubber is pre-treated by immersing them in a 2% polyvinyl alcohol solution for 30 min at room temperature. SFs (crimped with a length of 30 mm and an aspect ratio of 60) and PFs of length 12 mm are used as reinforcing fibres. The manufactured sand used in this study is replaced with crumb rubber.

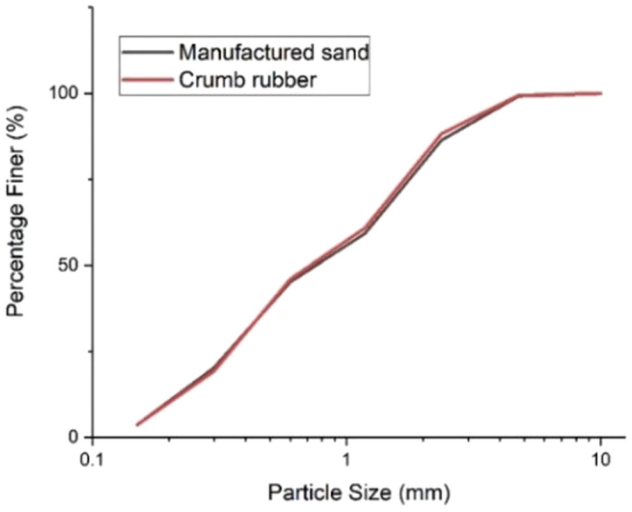

Figure 1: Particle size distribution of manufactured sand and rubber particles according to Long *et al.* [69].

Table 1: Proportion details of replacement materials for each mix variant [59]

Mix ID	Rubber (%)	SFs (%)	PFs (%)
R0	0	0	0
R5	5	0	0
R10	10	0	0
R15	15	0	0
R0SF0.25	0	0.25	0
R0SF0.5	0	0.5	0
R0SF0.75	0	0.75	0
R0SF1	0	1	0
R15SF0.75	15	0.75	0
R0PP0.1	0	0	0.1
R0PP0.2	0	0	0.2
R0PP0.3	0	0	0.3
R15PP0.2	15	0	0.2

Note: In R*X*, *X* is the percentage of replacement of fine aggregates with pre-treated crumb rubber. In SF*Y*, *Y* is the percentage volume of SF in the total volume of concrete. In PP*Z*, *Z* is the percentage volume of PF in the total volume of concrete.

The fine aggregates are replaced by 5, 10, and 15% with an equal volume of crumb rubber. The percentage replacement of mineral aggregates with crumb rubber is limited to 15% because beyond that considerable reduction in the compressive strength of concrete is noticed. The total volume of concrete is replaced with 0.25, 0.5, 0.75, and 1% SFs in SF-reinforced concrete. In the case of PF-reinforced concrete, the total volume of concrete is replaced with 0.1, 0.2, and 0.3% PFs. Tables 1 and 2 show the details of mix variants and constituent material proportions for various mixes [59]. The cost of materials used in the study is presented in Table 3 along with the details of embodied carbon of the constituent materials [59]. The environmental benefit of adopting fibre-reinforced RCSs is presented in Table 4. It should be noted that precious mineral aggregates can be saved using RCSs. Based on the mix proportions presented in Table 2, it is estimated that, for every kilometre of the track construction with fibre-reinforced RCSs, about 16 tonnes of manufactured sand can be saved, and 3.8 tonnes of crumb rubber (derived from waste tires) is used. Every kilogram of crumb rubber used is a kilogram of rubber removed from the waste disposal on land. Thus, effective recycling of waste tyre rubber particles can be achieved by adopting more RCSs or fibre-reinforced RCSs reinforced with steel or PFs. It is interesting

Table 2: Mix proportions of all constituent materials (in kg/m^3) [59]

Mix ID	Cem	Met	Sand	Crushed stones	Water	HR	VM	Rb	SF	PF
R0	441	41	670	1,191	162	4	2	0	0	0
R5	441	41	636	1,191	162	4	2	8	0	0
R10	441	41	603	1,191	162	4	2	16	0	0
R15	441	41	569	1,191	162	4	2	24	0	0
R20	441	41	536	1,191	162	4	2	33	0	0
R0SF0.25	440	41	668	1,189	161	4	2	0	20	0
R0SF0.5	439	40	668	1,188	161	4	2	0	39	0
R0SF0.75	438	40	667	1,187	161	4	2	0	59	0
R0SF1	437	40	666	1,185	160	4	2	0	79	0
R15SF0.75	438	40	567	1,187	161	4	2	24	59	0
R0PP0.1	441	40	669	1,191	162	4	2	0	0	1
R0PP0.2	440	40	669	1,190	161	4	2	0	0	2
R0PP0.3	440	40	669	1,189	161	4	2	0	0	3
R15PP0.2	440	40	569	1,190	161	4	2	24	0	2

Cem – Cement; Met – Metakaolin; HR – high-range water reducer; VM – viscosity-modifying agent; Rb – pre-treated crumb rubber; SF – steel fibre; PF – polypropylene fibre.

Table 3: Cost breakdown of constituent materials used

Materials	Unit cost (USD/kg)	Embodied carbon (kg CO_2/kg) [70–73]
Cement	0.117	0.912
Metakaolin	1.391	0.33
Rubber	0.582	−3.142
Manufactured sand	0.010	0.0027
Coarse aggregate	0.009	0.0027
Superplasticiser	1.676	0.72
SF	1.345	2.75
PF	4.365	2.7
Polyvinyl alcohol	9	1.71

to observe that the amount of embodied carbon is lower for RCS and PFRS by 17.80 and 16.82% when compared to that of ordinary concrete sleeper (OCS). This is mainly due to the negative value of embodied carbon for reused crumb rubber, which reduces the embodied carbon for these sleepers as indicated in Table 3. In contrast, the increase in the quantity of embodied carbon for SF-reinforced rubber concrete sleeper (SFRS) is 19% when compared to that of OCS. The higher magnitude of embodied carbon in the production of SF results in an increased cumulative magnitude of embodied carbon for SFRS.

The optimum proportions of pre-treated crumb rubber in rubber concrete, SFs in SF-reinforced concrete, and PFs in PF-reinforced concrete have been found initially by determining the cost-to-impact strength ratio. Drop weight impact tests have been carried out on prisms with 100 mm × 100 mm cross-section and 500 mm total length [18,40]. The effective length of the prisms was 400 mm. Multiple drops have been imparted on prisms using an impactor of mass 3.5 kg with a drop height of 100 mm. The tests can be concluded on the basis of the generation of cracks at the bottom of the prism. Eq. (1) can be used to determine their impact energy [74]:

$$\text{IE} = Nmgh, \tag{1}$$

where IE represents the impact energy in Nm, N stands for the number of blows till the appearance of cracks at the bottom of the prism, g is the acceleration due to gravity (9.81 m/s^2), and h signifies the height of fall in m.

As shown in Figure 2, the optimal proportion of replacement of manufactured sand with crumb rubber is around 15%. In SF-reinforced concrete, 0.75% SFs yield maximum impact energy to cost ratio. The minimum ratio of cost to impact energy for PF-reinforced concrete prisms was found to be 0.2%. Hence, detailed investigations can be carried out using the optimum proportions of crumb rubber, SFs, and PFs. Hereafter, the concrete without crumb rubber or fibres will be termed ordinary concrete. The concrete with crumb rubber will be referred to as rubber concrete. Concrete with rubber and fibre mix will be called SF-reinforced rubber concrete and PF-reinforced rubber concrete depending on the type of fibres present. The fibre-reinforced concrete will be noted as SF-reinforced concrete and PF-reinforced concrete based on the type of fibre included.

Concrete cylinders of 150 mm diameter and 300 mm depth are then subjected to compression in a displacement-controlled compression testing arrangement. Linearly varying displacement transducers have been attached to the specimens to measure vertical compression. Figure 3 depicts the results of the compression, flexural, impact energy, modulus of elasticity, and density tests on concrete [75,76]. The initial part of the stress–strain curves behaves linearly. The presence of voids imparted into the concrete matrix with the addition of crumb rubber particles plays a critical role in lowering the peak stress in rubber concrete specimens when compared to ordinary concrete specimens. For rubber concrete mixes, there is an increase in the strain corresponding to maximum stress due to the ability of rubber particles to elongate. Besides, the initial slope of the stress–strain curve of rubber concrete mixes is lower than the initial slope of conventional concrete mixes. When PFs are added to concrete, the changes in the initial slope of the stress–strain curve are not significant. This may be because of the nature of fibres that only prevents the shrinkage cracks in concrete. The ability of SFs to actively prevent the widening of generated cracks in concrete has resulted in improving the peak stress and increasing the strain corresponding to the SF-reinforced concrete specimen and SF-reinforced rubber concrete specimen. The strain corresponding to

Table 4: Environmental benefits of adopting fibre-reinforced RCSs

Sleeper type	Manufactured sand saved (t/km of track)	Crumb rubber used (t/km of track)	Embodied carbon (kg CO_2/km of track)	Percentage reduction in embodied carbon (kg CO_2/km of track)
OCS	0	0	—	—
RCS	15.99	3.8	55324.3	17.8
PFRS	16.3	3.8	55982.18	16.82
SFRS	15.91	3.8	80525.69	−19.63

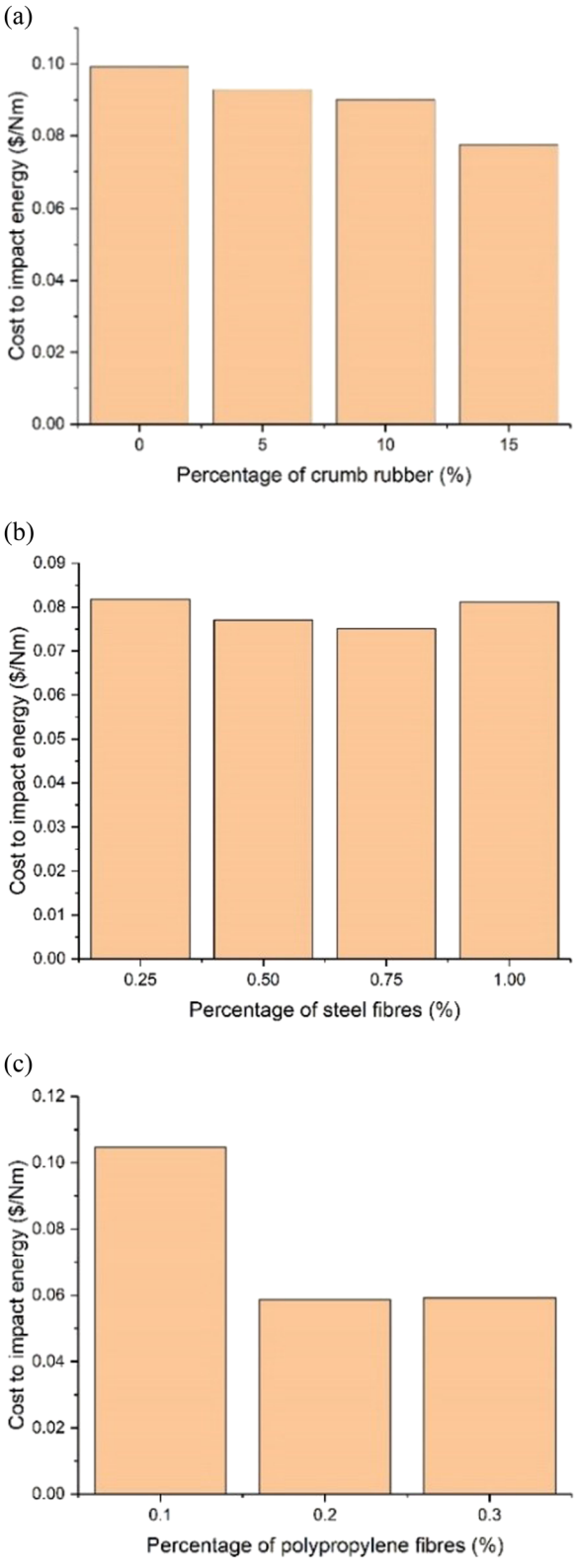

Figure 2: Cost to impact energy for (a) rubber concrete prisms, (b) SF-reinforced concrete prisms, and (c) PF-reinforced concrete prisms.

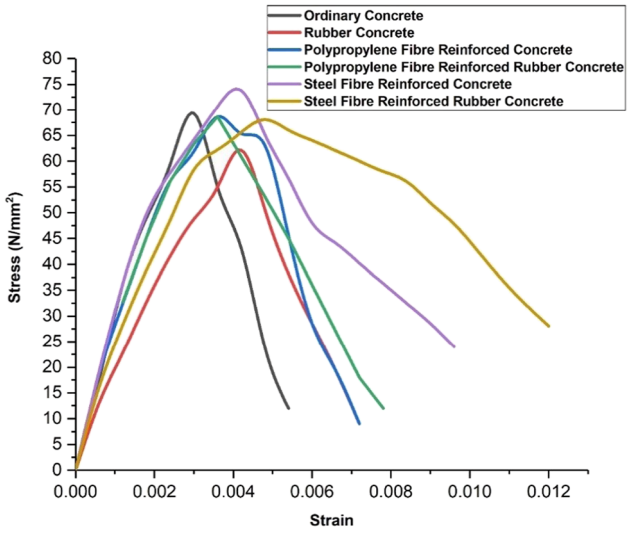

Figure 3: Stress–strain curves of materials used for sleepers.

peak stress is greater than the ordinary concrete specimen. The use of SFs also causes the initial slope of the stress–-strain curve steeper when compared to that of ordinary concrete specimens. This study primarily focuses on utilizing the values of the static modulus of elasticity for different materials (Figure 3) and its strain rate-dependent variation discussed in Section 3 for the simulation of train motion. The modulus of elasticity obtained is later utilized as a material property for the different sleepers studied. Table 5 shows the engineering properties of the mixes [59].

2.1 Finite element (FE) model

The numerical analysis of the ballasted track structure is carried out using the FE software LS-DYNA. The modelling of the ballasted railway track is carried out based on previous work [63,64]. The ballasted railway track's FE model comprises rail, rail pad, sleeper, ballast, sub-ballast, and subgrade. China Railway High Speed (CRH) 2 Electric Multiple Unit (EMU) train is used to carry out the study [54]. The TRACK and TRAIN keywords of the RAIL module assist in the simulation of train motion over rails. Mesh convergence is carried out by varying the mesh sizes of the track components. After the mesh convergence studies, the LS-DYNA model contains 64,472 elements (586 beam elements, 312 discrete elements, 60 shell elements, and 63,514 solid elements). The element size of the rail is 0.165 m. The dimension of the solid element used for the sleeper varies from 0.1135 m × 0.2665 m × 0.06 m to 0.1135 m × 0.359 m ×

Table 5: Engineering properties of concrete

Mix designation	f_c	f_t	I.E	E	ρ
R0	69	5.83	520.91	2.93×10^{10}	2,511
R15	62	4.98	725.80	1.78×10^{10}	2,476
R0PP0.2	68	5.78	923.75	3.04×10^{10}	2,508
R15PP0.2	63	5.47	1157.08	2.67×10^{10}	2,432
R0SF0.75	74	6.35	1041.82	3.31×10^{10}	2,551
R15SF0.75	68	5.85	1620.61	2.31×10^{10}	2,476

f_c – compressive strength (in N/mm^2), f_t – flexure strength (in N/mm^2), IE – impact energy (in Nm); E – modulus of elasticity (in Pa), ρ – density (in kg/m^3).

0.06 m. The maximum size of the solid element used for ballast is 0.105 m × 0.359 m × 0.175 m. The size of the element used as a sub-ballast is limited to 0.105 m × 0.359 m × 0.1 m, whereas the maximum size of the element used to model the subgrade is 0.105 m × 0.359 m × 0.2 m.

The dynamic rail pad stiffness has been introduced by providing a rail pad stiffness value of 50 kN/mm. The variation in the modulus of elasticity due to the effect of strain rate has been explored by many researchers [65,77,78]. The enhancement factors for strain rate proposed by Comite Euro-International Du Beton are presented in Eqs. (2) and (3) [79]:

$$\eta_c = \frac{E_d}{E_s} = \left(\frac{\dot{e}}{\dot{e}_{sc}}\right)^{0.026}, \tag{2}$$

$$\eta_t = \frac{E_d}{E_s} = \left(\frac{\dot{e}}{\dot{e}_{st}}\right)^{0.016}, \tag{3}$$

where η_c and η_t are the enhancement factors for the strain rate in compression and tension. E_d and E_s represent the dynamic and static modulus of elasticity. The effective strain rate of concrete under dynamic load is $\dot{e}$. The effective strain rate of concrete under tensile and compressive loads is denoted by $\dot{e}_{st}$ and $\dot{e}_{sc}$, respectively. It should be noted that $\dot{e}_{st}$ and $\dot{e}_{sc}$ take up values 3×10^{-6} and 30×10^{-6}/s, respectively.

The Winfrith concrete model proposes the use of average strain rate enhancement factors, and the following equation is used to relate the dynamic modulus of elasticity and strain rate [65,77,78]:

$$\frac{E_d}{E_s} = 0.5 \times \left[\left(\frac{\dot{e}}{3 \times 10^{-6}}\right)^{0.016} + \left(\frac{\dot{e}}{30 \times 10^{-6}}\right)^{0.026}\right]. \tag{4}$$

The dynamic strain rate model is used to implement the strain rate-dependent plasticity property in concrete sleepers. The variation in the enhancement factor with a change in the strain rate is presented in Figure 4. The minimum value of the enhancement factor is taken as 1.

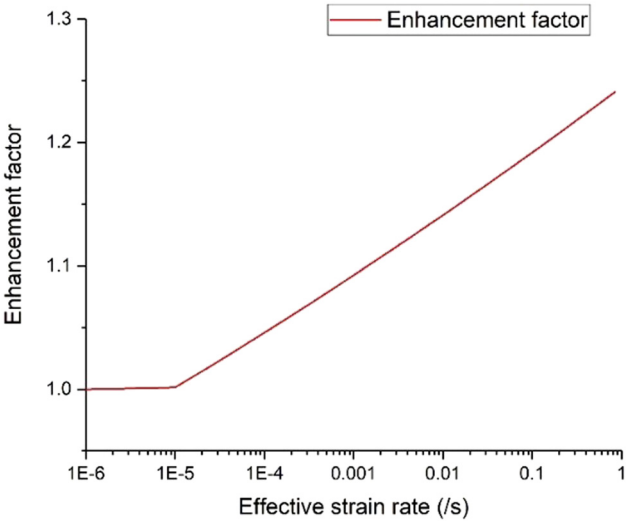

Figure 4: Relation between the enhancement factor and effective strain rate.

The dynamic modulus of elasticity and yield stress, presented as a function of the strain rate from the input of the keyword STRAIN_RATE_DEPENDENT_PLASTICITY, is used to introduce the strain rate enhancement effect on concrete sleepers. The yield stress used in the model is taken from Table 5. The trains' motion has been described by the command PRESCRIBED_MOTION_RIGID module. The wheel–rail interactions are excited using the German high-speed low-disturbance irregularity. The power spectrum density function, which defines the wheel–rail contact surface irregularity, is presented in Eq. (5):

$$S_v(\Omega) = \frac{A_v \Omega_c^2}{(\Omega^2 + \Omega_c^2)(\Omega^2 + \Omega_r^2)}. \tag{5}$$

$S_v(\Omega)$ represents the vertical power spectral density, and the roughness constant $A_v = 4.032 \times 10^{-7}$ m^2 rad/m. The spatial frequency of irregularities is denoted by Ω. The cut-off frequencies Ω_c and Ω_r are 0.8246 and 0.0206 rad/m, respectively. The velocity of the train varies from 50 to 250 kmph with an increment of 50 kmph. The validation of the track structure model has been robustly carried out using a train velocity of 250 kmph. The dimensions of the sleeper used in the model are 2.5 m × 0.227 m × 0.18 m. Properties of the track structure used are presented in Tables 6 and 7. Figures 5–7 present the details of the railway track structure simulated using FEA.

The numerical model has been fully validated using both experimental and numerical results presented by Zhang *et al.* [80] and China [81]. This numerical model exhibits a good agreement with the field observations, and the simulated results presented by researchers are shown in Table 8 and Figure 8.

Table 6: Mechanical properties of the train

Properties	Value [62]
Mass of the car body (kg)	4×10^4
Mass of the bogie (kg)	3.5×10^3
Mass of the wheelset (kg)	2×10^3
Moment of inertia of the bogie about the *x*-axis (kg/m^2)	2.6×10^3
Moment of inertia of the bogie about the *y*-axis (kg/m^2)	1.8×10^3
Moment of inertia of the wheelset (kg/m^2)	1×10^3
Stiffness of the primary suspension (N/m)	1.2×10^6
Damping of the primary suspension (N s/m)	2×10^4
Stiffness of the secondary suspension (N/m)	2×10^5
Damping of the secondary suspension (N s/m)	4×10^4

Table 7: Engineering properties of track constituents

Track component	Density (kg/m^3)	Modulus of elasticity (Pa)	Poisson's ratio
Rail	7,830	2×10^{11}	0.3
Ballast	1,590	9.7×10^7	0.12
Sub-ballast	1,910	2.12×10^8	0.2
Subgrade	2,300	2×10^8	0.25
OCS	2,511	2.933×10^{10}	0.2
RCS	2,476	1.78×10^{10}	0.2
PFCS	2,508	3.04×10^{10}	0.2
PFRS	2,432	2.67×10^{10}	0.2
SFCS	2,551	3.31×10^{10}	0.2
SFRS	2,476	2.31×10^{10}	0.2
Rail pad stiffness	5×10^7 N/m		
Rail pad damping	7.50×10^4 N s/m		

3 Results and discussion

The OCS, pre-treated crumb RCS, PF-reinforced concrete sleeper (PFCS), PFRS, SF-reinforced concrete sleeper (SFCS), and SFRS have been systemically considered in the unprecedented investigations into dynamic behaviours of ballasted railway tracks taking into account dynamic and strain-rate effects. Free vibration responses of railway sleepers are first identified using modal analyses. The sensitivity of train accelerations, rail displacements in the vertical direction, sleeper displacements, and ballast stresses are assessed to derive new nonlinear dynamic phenomena of the railway tracks when different types of sleepers are adopted. This section highlights new insights obtained during the investigations into the applications of fibre-reinforced RCSs to ballasted railway tracks.

3.1 Sleeper-free vibration responses

Herein, we first identify free vibration response characteristics of different types of railway concrete sleepers on the basis of eigenvalue analysis. This method is essential in understanding the dynamic behaviours of the track systems and in assessing the locations that are most susceptible to vibrations. It should be noted that the sleeper models used in this section have been validated with full-scale experiments derived from our previous works using a non-destructive test called the impact hammer excitation technique [8]. The fundamental mode shapes and corresponding frequencies of OCS have been obtained *via* the frequency response function. In this study, the properties of different types of sleepers obtained from the previous section are then applied in the model to investigate the

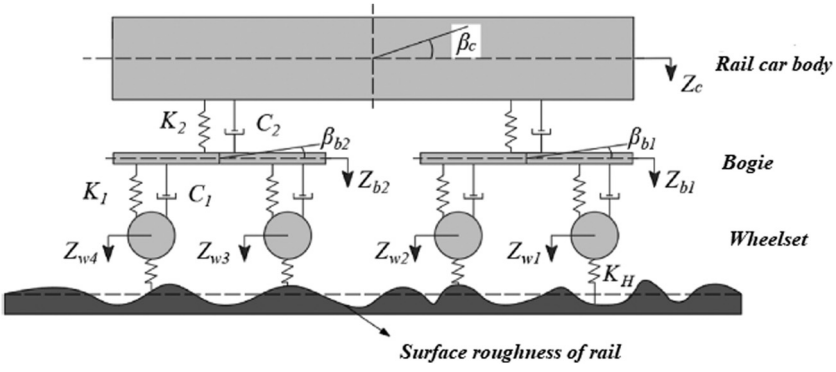

Figure 5: Sample model of the train.

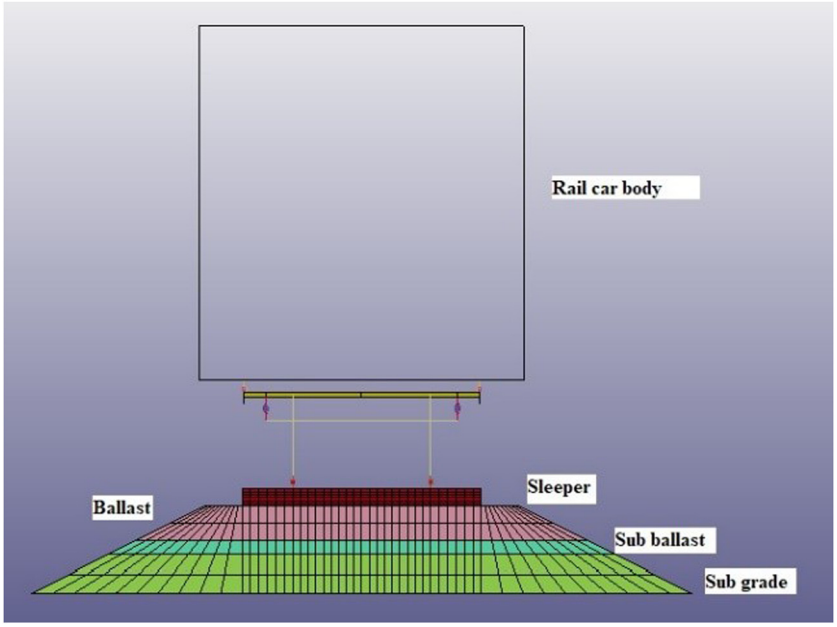

Figure 6: FE model of the track.

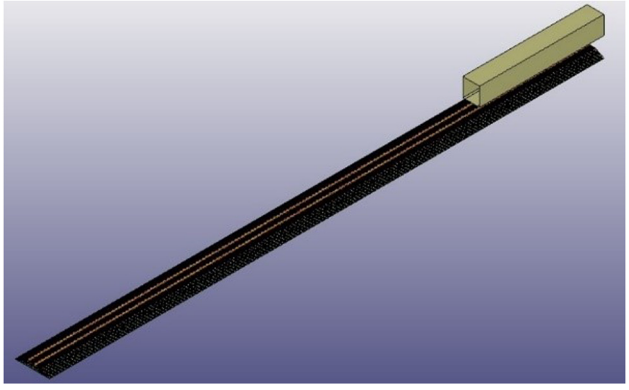

Figure 7: Numerical model.

influence of sleeper types on free vibration responses. The free–free condition is set as a boundary condition in the analysis to comply and validate with the experiment testing. It is important to note that free–free boundary condition presents a system that is not constrained in any direction and thus the sleepers can move freely with no effects of support conditions. Figure 9 presents the fundamental mode shapes of OCS. Only the bending and twisting modes are presented.

Table 9 compares the natural frequencies of the first six modes of different railway sleepers. It is seen that modes 1–4 of all sleepers are relatively similar, while modes 5–6 are not as the fourth bending mode of the RCSs and SFRSs has a higher frequency than the second twisting mode. It can be clearly seen that the natural frequencies of RCSs are the lowest with about 20% reduction compared with OCSs. It is followed by SFRSs with about 10% reduction. It is because the bending stiffness of those types is significantly decreased as the sleepers are softened even if the density is increased. Even though rubber is likely to better absorb vibration and impact, this makes the track more susceptible to vibration and deformation. However, adding SF in concrete sleepers can significantly increase natural frequencies leading to improving dynamic behaviours of railway sleepers.

Table 8: Cross-validation of the model with experimental and numerical results

Result	Experimental [80]	Numerical [81]	Present study
Maximum rail displacement (mm)	0.96	0.92	1.02
Maximum sleeper amplitude (mm)	0.42	0.39	0.37
Maximum rail acceleration (g)	32		30

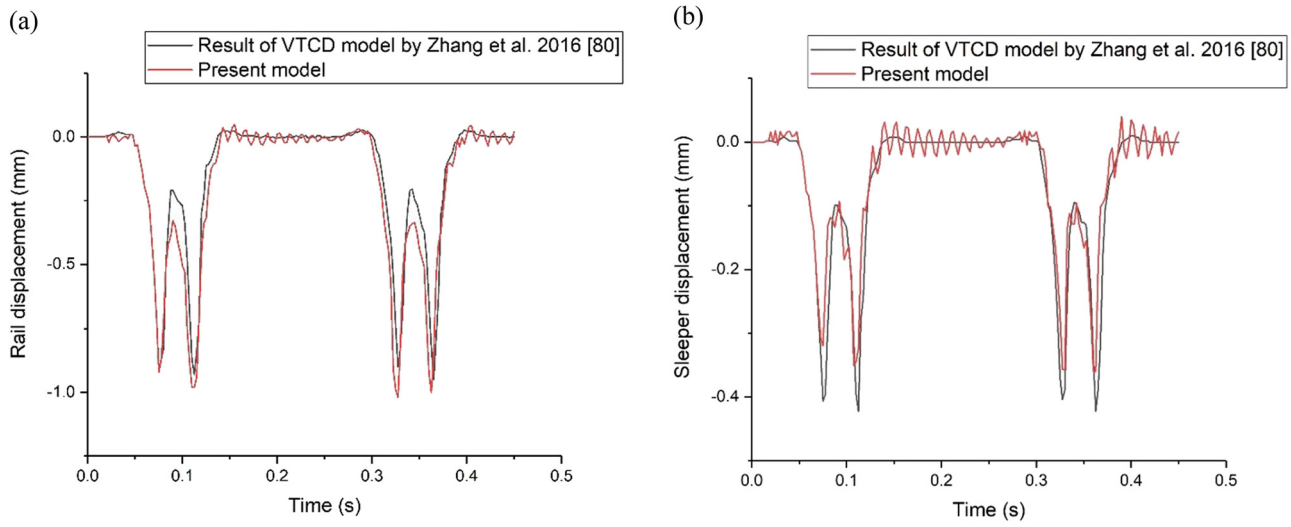

Figure 8: Comparison of dynamic rail and sleeper displacements for validations: (a) rail displacement comparison and, (b) sleeper displacement comparison.

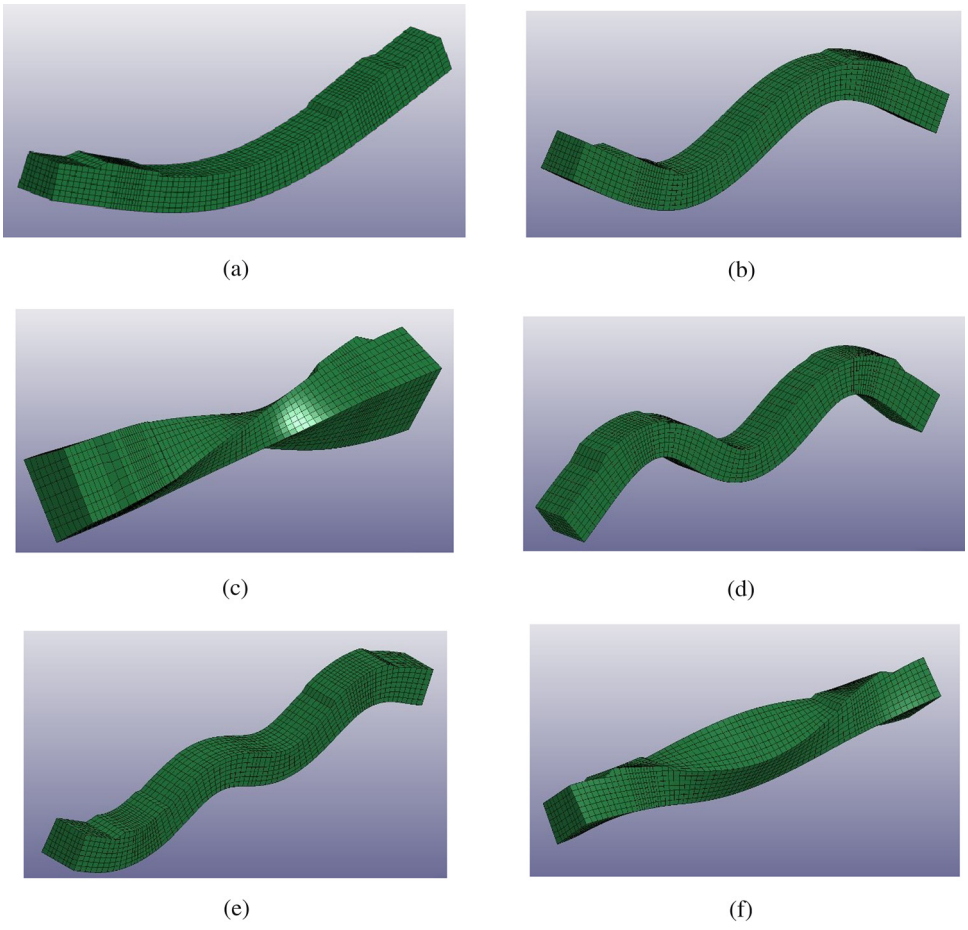

Figure 9: Corresponding mode shapes of an OCS (a) Mode 1 (1st bending), (b) Mode 2 (2nd bending), (c) Mode 3 (1st twisting), (d) Mode 4 (3rd bending), (e) Mode 5 (4th bending), and (f) Mode 6 (2nd twisting).

Table 9: Natural frequencies of railway sleepers (in Hz)

Sleeper types	Mode 1 (1st bending)	Mode 2 (2nd bending)	Mode 3 (1st twisting)	Mode 4 (3rd bending)	Mode 5 (4th bending)	Mode 6 (2nd twisting)
OCS	85.64	238.9	339	463.56	731.01	732.84
RCS	67.92	189.3	266	366.84	578.05	574.89
	(−20.69%)	(−20.76%)	(−21.53%)	(−20.86%)	(−20.92%)	(−21.55)
PFCS	87.23	243.24	345.37	472	744.329	746.53
	(+1.86%)	(+1.82%)	(+1.88%)	(+1.82%)	(+1.82%)	(+1.87%)
PFRS	83.14	231.86	328.61	449.83	709.27	710.29
	(−2.92%)	(−2.95%)	(−3.06%)	(−2.96%)	(−2.97%)	(−3.08%)
SFCS	90.11	251.39	357.37	487.92	769.51	772.48
	(+5.22%)	(+5.23%)	(+5.42%)	(+5.25%)	(+5.27%)	(+5.41%)
SFRS	76.92	214.39	302.99	415.77	655.42	654.89
	(−10.18%)	(−10.26%)	(−10.62%)	(−10.31%)	(−10.34%)	(−10.64%)

(−): indicates percentage variation with respect to OCS.

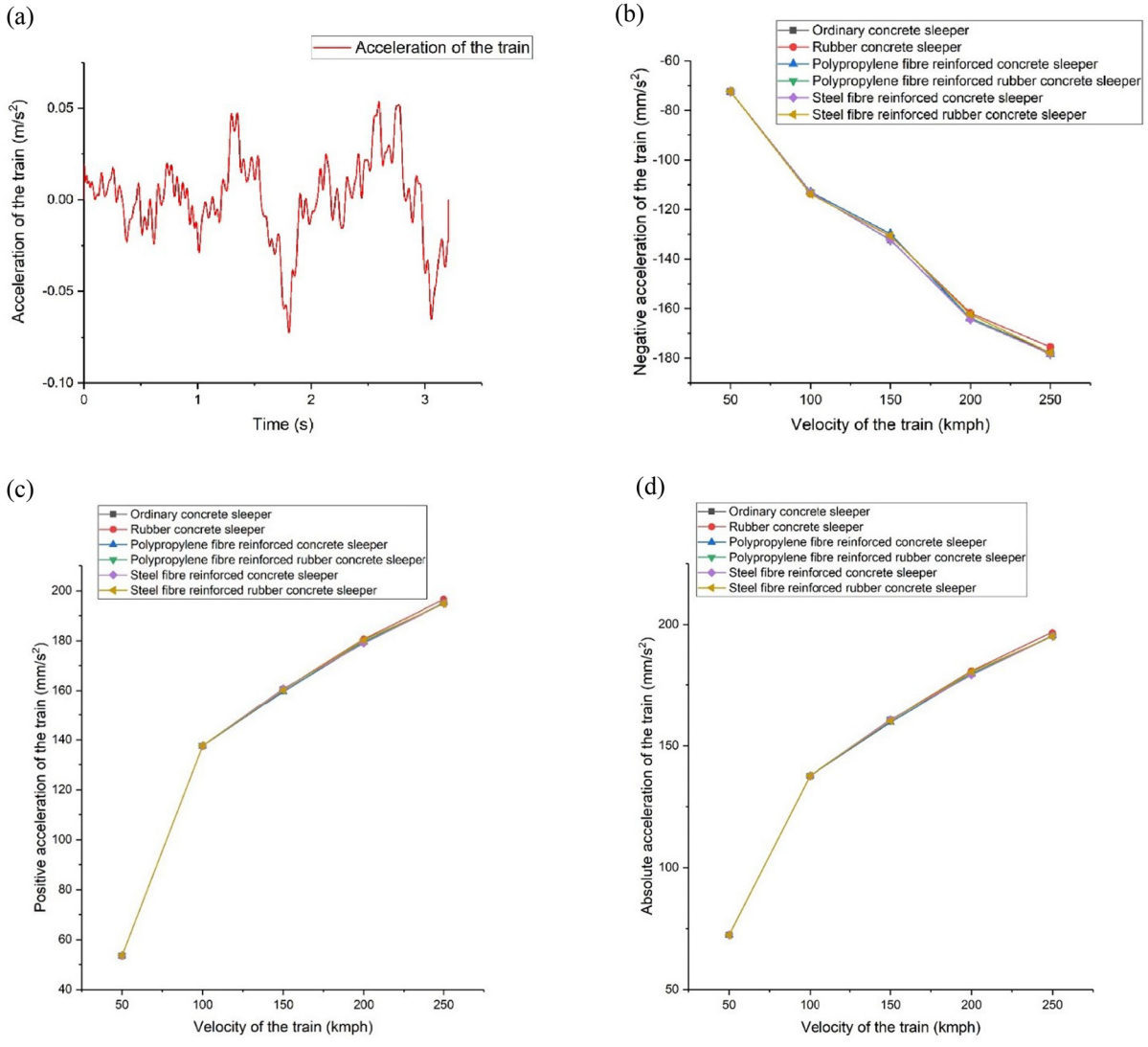

Figure 10: Accelerations of the train body: (a) accelerations of the train body with a velocity of 50 kmph for ordinary concrete, (b) negative accelerations of the train body, (c) positive accelerations of the train body, and (d) absolute accelerations of the train body.

3.2 Train–track analysis

3.2.1 Train vibration

Figure 10 shows the characteristics of vertical accelerations of the train body. When different types of sleepers are introduced, the acceleration trends seem to be similar. The trend of maximum negative acceleration across varying train velocities indicated that maximum acceleration increases with an increase in velocity. The consistent increase in the magnitude of maximum negative acceleration together with the increase in train velocity may be attributed to increasing vibrations of the track structure. It is evident from Figure 10 that the changes introduced to railway sleepers are inconsequential to the acceleration of the train body and resultant ride comfort. However, it is noticeable that the magnitude of the maximum negative acceleration of the train body when adopting RCSs is slightly lower at a velocity of 250 kmph when compared to other types of railway sleepers.

3.2.2 Dynamic rail responses

The dynamic displacements and uplifts of the rails are presented in Figures 11–13. It can be noted that the vertical displacements increase with an increase in the train velocity. The use of RCS induces maximum rail displacements for all ranges of train velocities when compared to other types of railway sleepers.

Figure 12 presents the details of maximum dynamic rail displacements in the downward direction. The maximum rail displacement of 1.0447 mm is noted for RCS when the train velocity is at 250 kmph. The increase in rail displacements is about 1.5% when RCS is introduced in place of OCS. It can also be noticed that the minimum displacement in rails can be noticed for SFCS. The variations in dynamic rail displacements for PFCS, PFRS, and SFRS are similar to those of the OCS.

Figure 13 depicts the dynamic characteristics of upward deflection to the rail's so-called "up-lift" in the ballasted tracks. The uplift occurs generally away from the concentrated location of wheelsets due to the bending behaviour of the rail caused by the motion of the train. It is interesting to note that the minimum rail uplift occurs at a train velocity of 100 kmph and remains almost constant up to a train velocity of 150 kmph. But when compared to the initial velocities, the uplifts of rail still incur with a more significant magnitude at train velocities greater than 200 kmph. The increase in rail uplifts can be clubbed together with the magnitude of the negative acceleration of the train as the trends in their variation

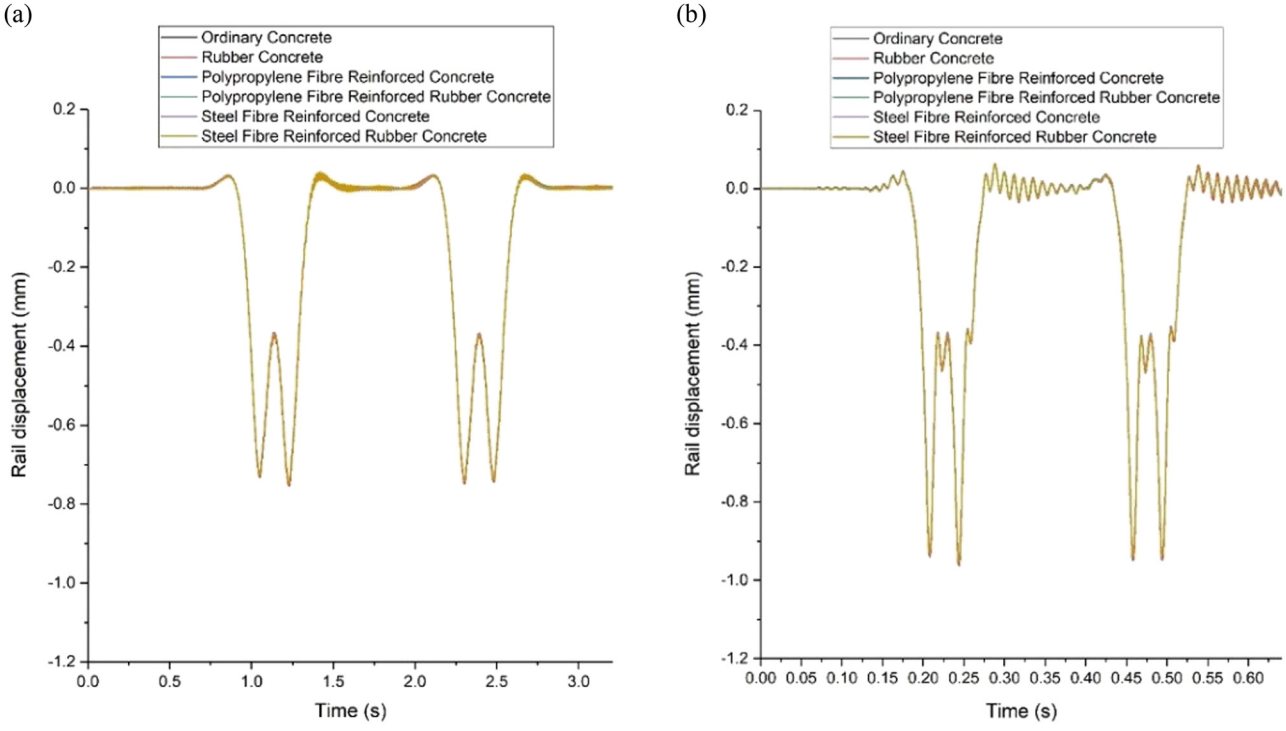

Figure 11: Dynamic rail displacement variation when different sleepers are used. Rail displacements (a) at 50 kmph and (b) at 250 kmph.

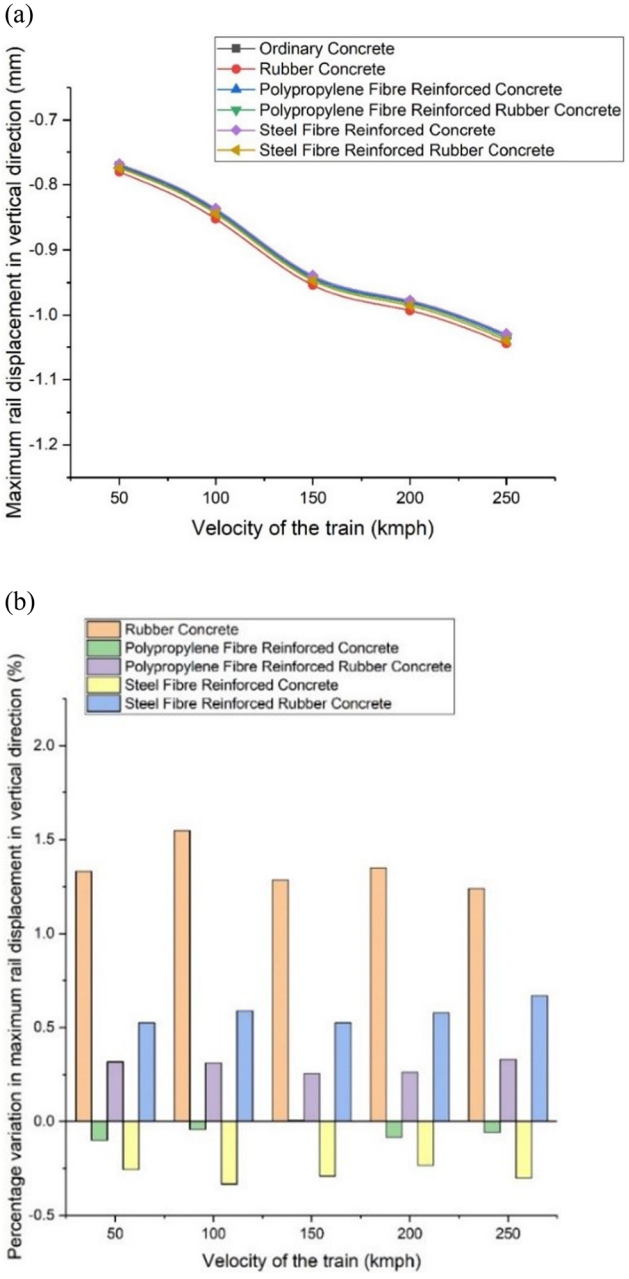

Figure 12: Maximum dynamic rail displacements in the downward direction: (a) maximum rail displacement and (b) percentage variation in maximum rail displacement.

are similar. Nowadays, the maximum operational safety limit of vertical displacement is kept at 2 mm [82]. In that aspect, it is to be noted that when the sleepers considered in this study are used, the maximum vertical displacement of rail is lower than 1.05 mm, which satisfies the operational safety requirement.

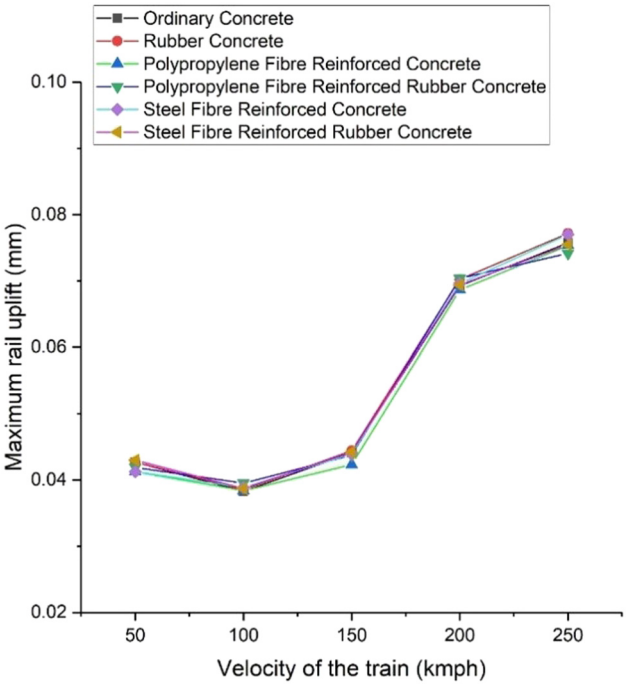

Figure 13: Maximum dynamic rail uplifts.

3.2.3 Sleeper responses

Dynamic vertical displacements at the rail seats of the sleepers and the centre of the sleepers have been evaluated since they can affect the differential track geometry and ride comfort. Figure 14 presents the time history plot of displacement at the rail seat of the sleeper.

It is noticeable from Figures 14 and 15 that as the train velocity increases, the downward vertical displacement of the sleeper at the rail seat increases. The rail seats of the RCS displace 5.5% more in the downward direction when compared to the OCS. A maximum rail seat sleeper displacement of −0.37801 mm can be noticed when RCS is used. When SFCSs are used, the rail seat sleeper displacements become −0.36204 mm. The minimum displacements at the rail seat locations of the sleepers can be observed when SFCSs are adopted. The presence of pores in rubber concrete when compared to ordinary concrete has led to a decrease in the load-carrying capacity of rubber concrete. As a result, about a 4.8–5.5% increase in sleeper displacements at rail seats can be noticed when RCSs are used instead of OCS concrete sleepers when SFCSs are used. In the case of railway tracks in which PFRS are used, the sleeper displacements at the rail seats are higher when compared to that of PFCS by 0.3 1.3%. The increasing trend

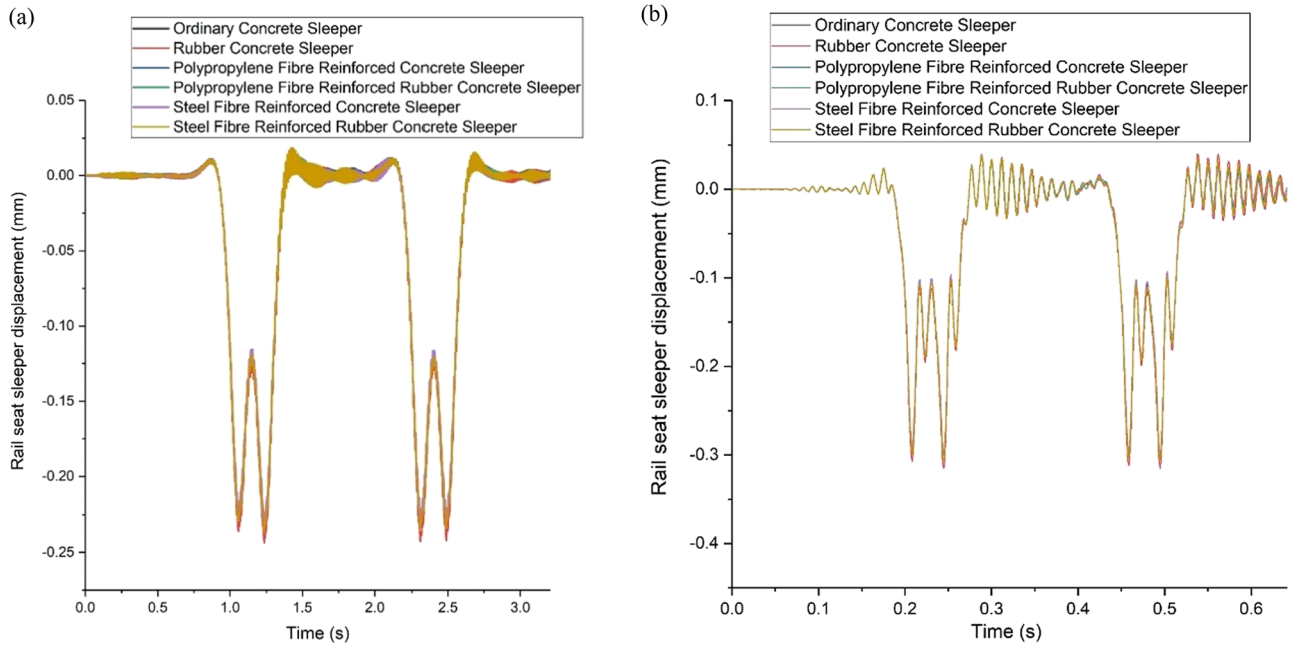

Figure 14: Dynamic rail seat sleeper displacements. Rail seat sleeper displacements (a) at 50 kmph and (b) at 250 kmph.

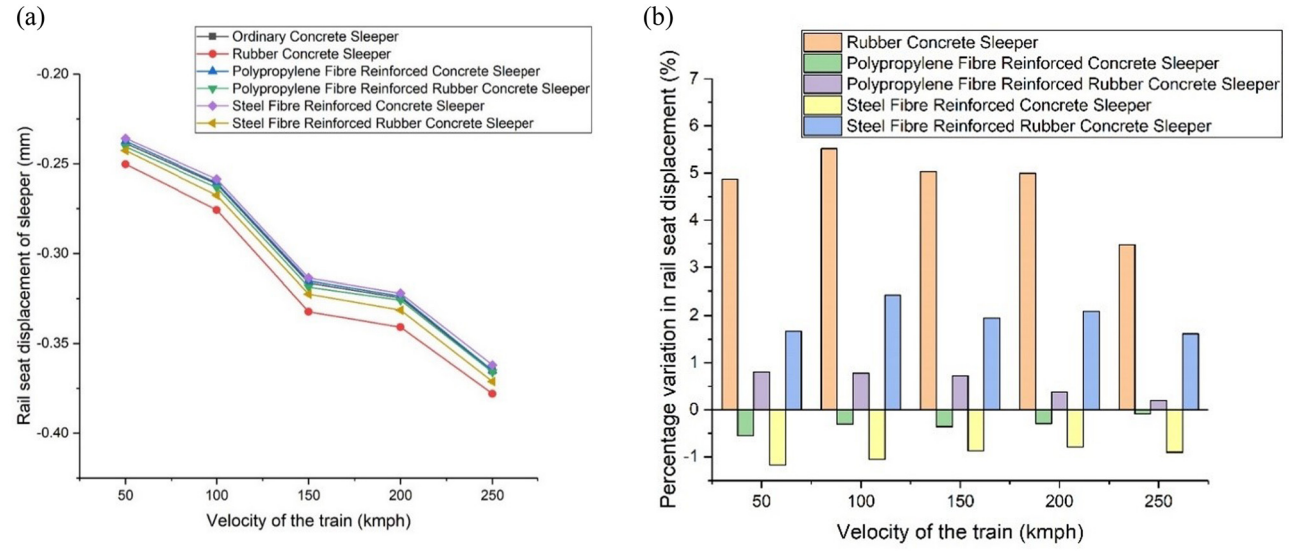

Figure 15: (a) Maximum dynamic rail seat sleeper displacements. (b) Percentage variation in maximum dynamic rail seat sleeper displacements.

in rail seat sleeper deflections with a decrease in compression moduli (modulus of elasticity) and *vice versa* is along with those presented by Salih *et al.* [83]. However, considering the significant decrease in the compression modulus for rubber concrete when compared to ordinary concrete, its dynamic characteristics have helped in keeping the increase of rail seat displacements to a lower level of 5% as can be seen in Figures 15 and 16. The rail seat displacements of SFRS are thus comparable to that of OCS. The improved performance of fibre-reinforced concrete sleepers in rail seat displacement can be attributed to the action of fibres which add rigidity to the concrete matrix by holding the inherent defects in concrete from falling apart. However, the rigidity imparted by the SFs to the concrete reduced its damping characteristics and the lowering of rail seat displacement is a mere 1% when SFCSs are adopted. As shown in Figure 16, the peak amplitudes of acceleration for SFCSs are greater than other types of railway sleepers.

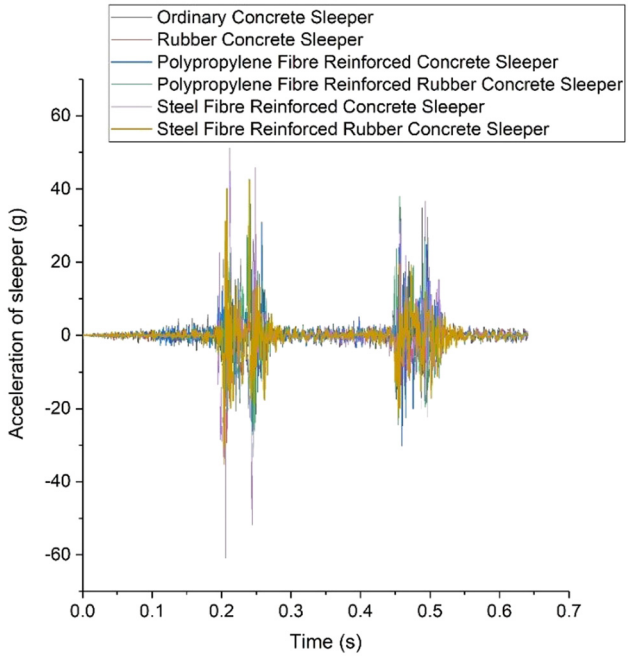

Figure 16: Representation of accelerations of railway sleepers at a train velocity of 250 kmph.

Figure 16 shows the representative accelerations of sleepers at a train velocity of 250 kmph. It should be noted that the minimum amplitude of accelerations can be seen for RCS. It indicates that rubber concrete can reduce the vibrations of sleepers. It should also be noted that the maximum amplitude of accelerations can be vividly noticed for SFCS. This susceptibility to vibration has resulted in only minor improvement in sleeper rail seat deflections for SFCS, despite having a relatively higher compressive strength and compression modulus of elasticity. Thus, it clearly reveals that RCS and fibre-reinforced RCSs perform better when subjected to dynamic loads, despite having a lower modulus of elasticity when compared to the concrete and fibre-reinforced concrete sleepers. This is also an important insight for practicing engineers to note that the vibrations are damped out at a faster rate for rubber concrete and fibre-reinforced RCSs when compared to their traditional high-strength concrete counterparts due to their higher damping ratio when compared to that of concrete and fibre-reinforced concrete sleepers.

Figure 17 presents the variation in sleeper centre displacements *versus* train velocities for different sleepers used. It can be found that the relative tendency is the opposite of that of rail seat displacements. The trend in sleeper centre displacement can be associated with the "w" shape of the critical mode shape of the sleepers [83]. This is a new finding to demonstrate that the third bending mode will play a key role in the structural condition

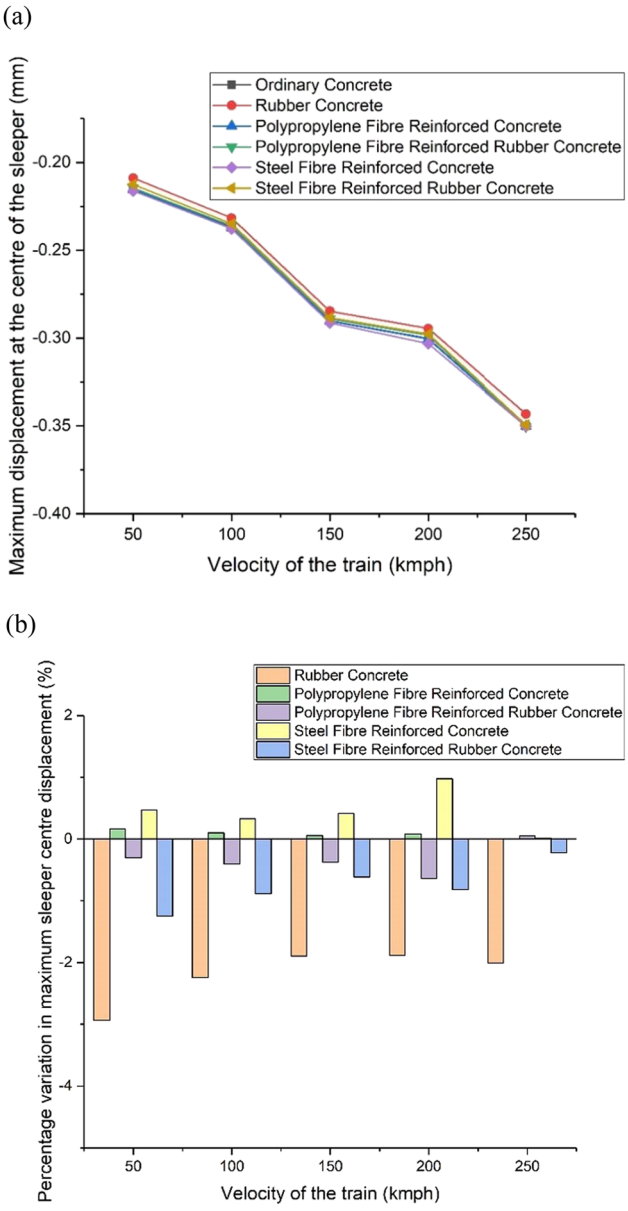

Figure 17: Maximum dynamic sleeper centre displacements: (a) variation in maximum sleeper centre displacements with train velocity and (b) percentage variation in sleeper centre displacements with respect to OCSs.

of sleepers at the mid-span. The trend in sleeper displacements indicates that a higher rail seat displacement is associated with a comparatively lower sleeper centre displacement. A minimum displacement at the sleeper centre can be clearly noted for RCS. The sleeper centre displacements are 2.5% lower, when RCS is used and when compared to OCS. The sleeper centre displacements of PFRS and SFRS are about 1% lower than that of OCS. SFCSs have undergone the maximum displacement. When SFCSs are utilized, an increase in sleeper centre displacements can be vividly noticed when compared to OCS.

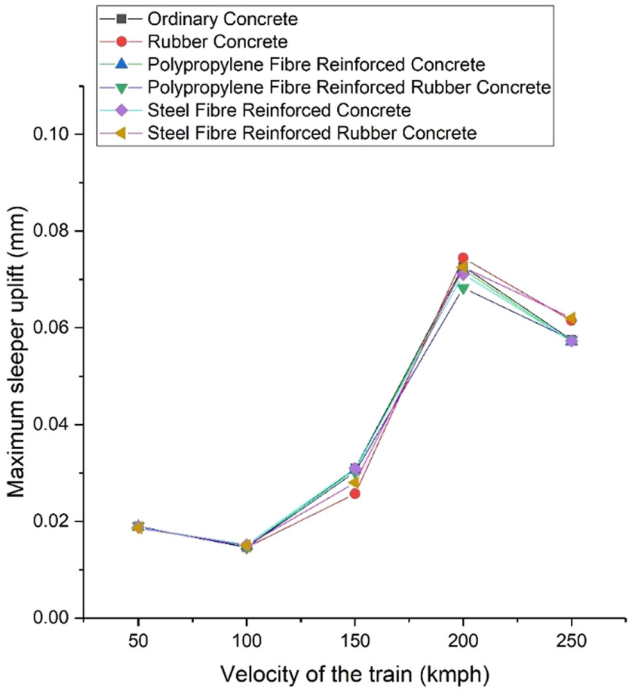

Figure 18: Maximum sleeper uplift.

The maximum allowable displacement in a sleeper is limited to 5 mm [82]. In the case of sleepers presented in this study, the maximum displacement undergone by the sleepers was 0.38 mm. Hence, it can be safely ascertained that all the sleepers evaluated have performed within the permissible limits (the maximum displacement encountered is lower than the maximum permissible displacement).

Figure 18 presents the variation in maximum sleeper uplifts for different cases studied herein. It can be noticed that the peak uplift of sleepers can be observed at a train velocity of 200 kmph. The sleeper uplifts in the case of RCS are minimum for lower train velocities up to 150 kmph. Above 150 kmph, the dynamic uplifts of RCS slightly increase above the other sleepers. The peak uplifts at 200 kmph are contributed by the resonance of frequencies of vibrations, and can potentially cause rapid ballast breakages, track geometry deterioration, and different track settlements.

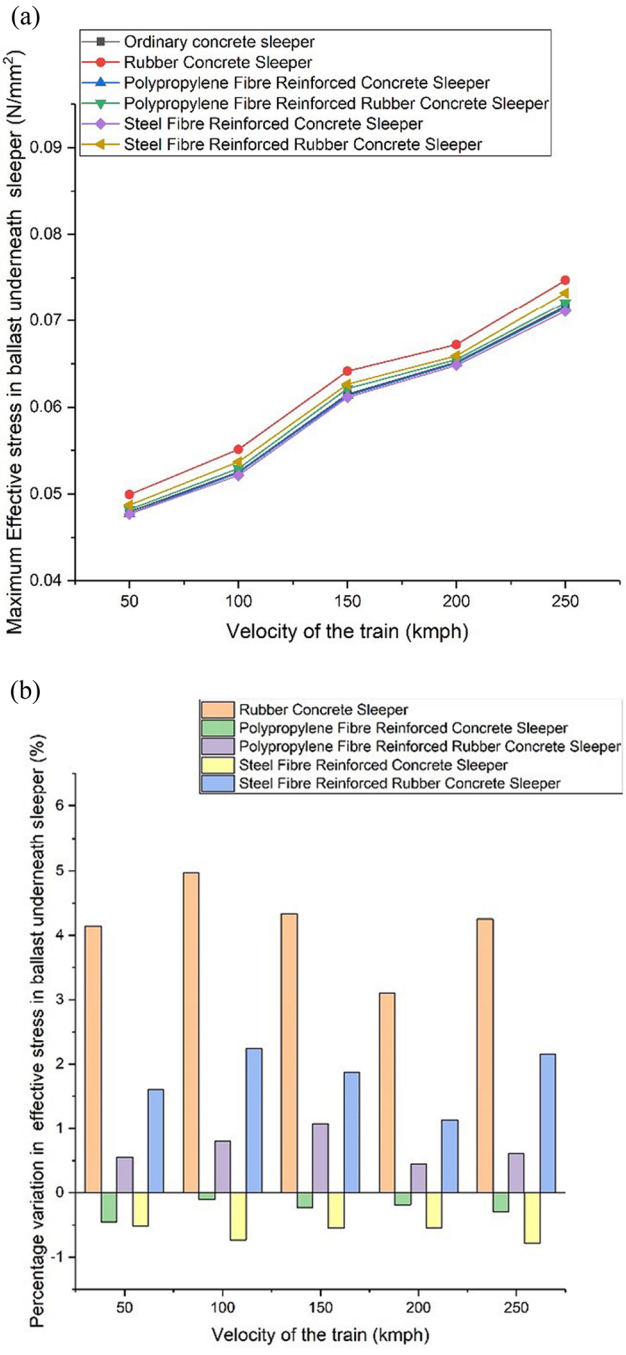

Figure 19: Effective stresses in ballast: (a) effective stresses in ballast under sleeper and (b) variation in effective stresses in ballast under sleeper.

3.2.4 Ballast responses

One of the major functions of railway sleepers is to transfer the load from the train wheels to the underlying ballast and foundation. The effective stresses withstood by the ballast indicate the intensity of dynamic load transferred to the ballast by the sleepers. Our findings provide new evidence to demonstrate that, under dynamic load conditions, the deformation of ballast underneath the sleepers is not uniform across the length of the sleeper. In the case of the most critical mode shape of sleepers (w-shape), the area of ballast underneath the rail seats undergoes higher displacement when compared to that below the sleeper centre.

Figure 19 shows the effective stresses under the rail seats of the sleeper for the most critical mode shape of the sleeper. Effective stresses in ballast are dependent on the

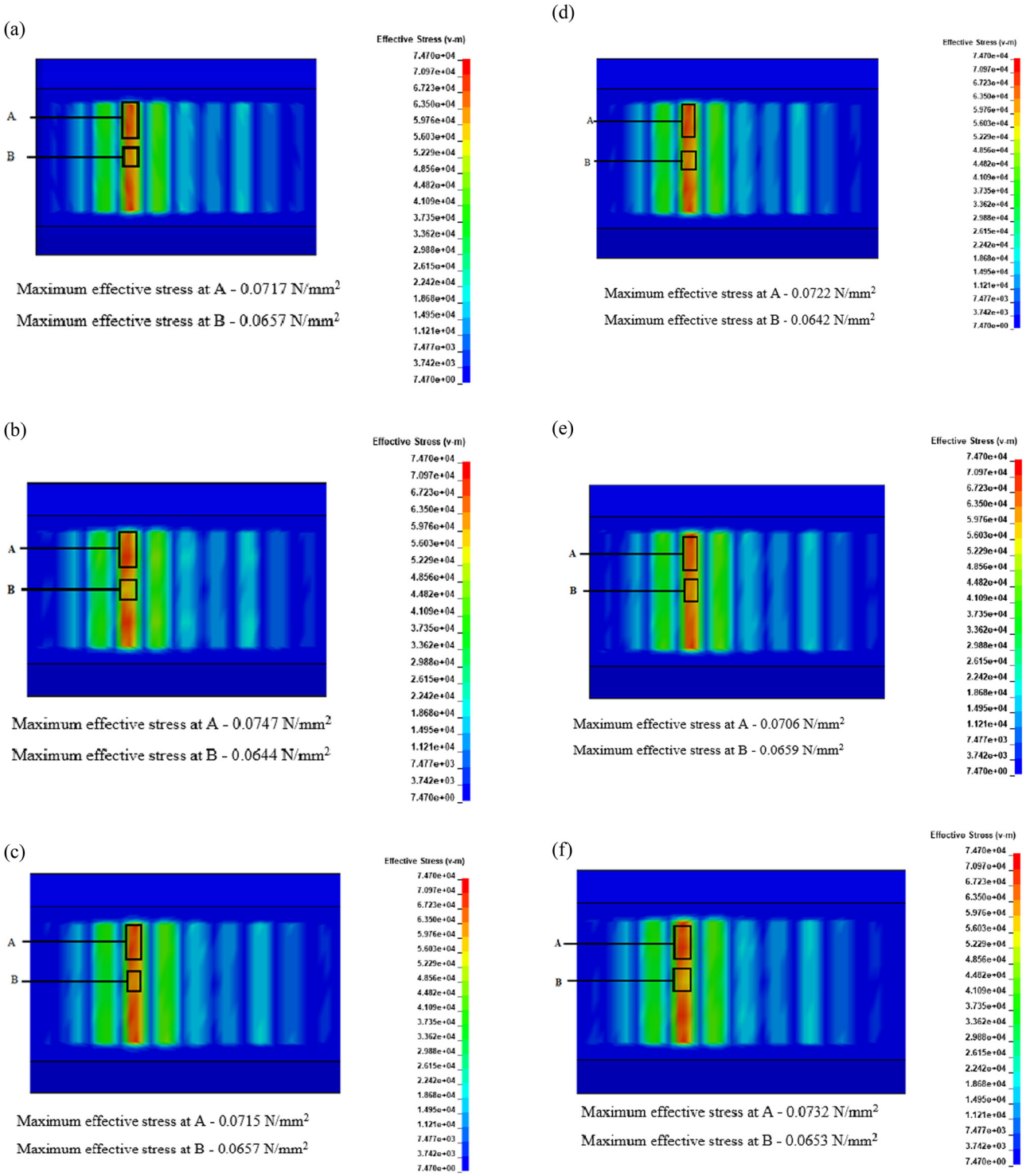

Figure 20: Variation in effective stresses in ballast at a train velocity of 250 kmph in ballasted railway tracks with (a) OCS, (b) RCS, (c) PFCS, (d) PFRS, (e) SFCS, and (f) SFRS.

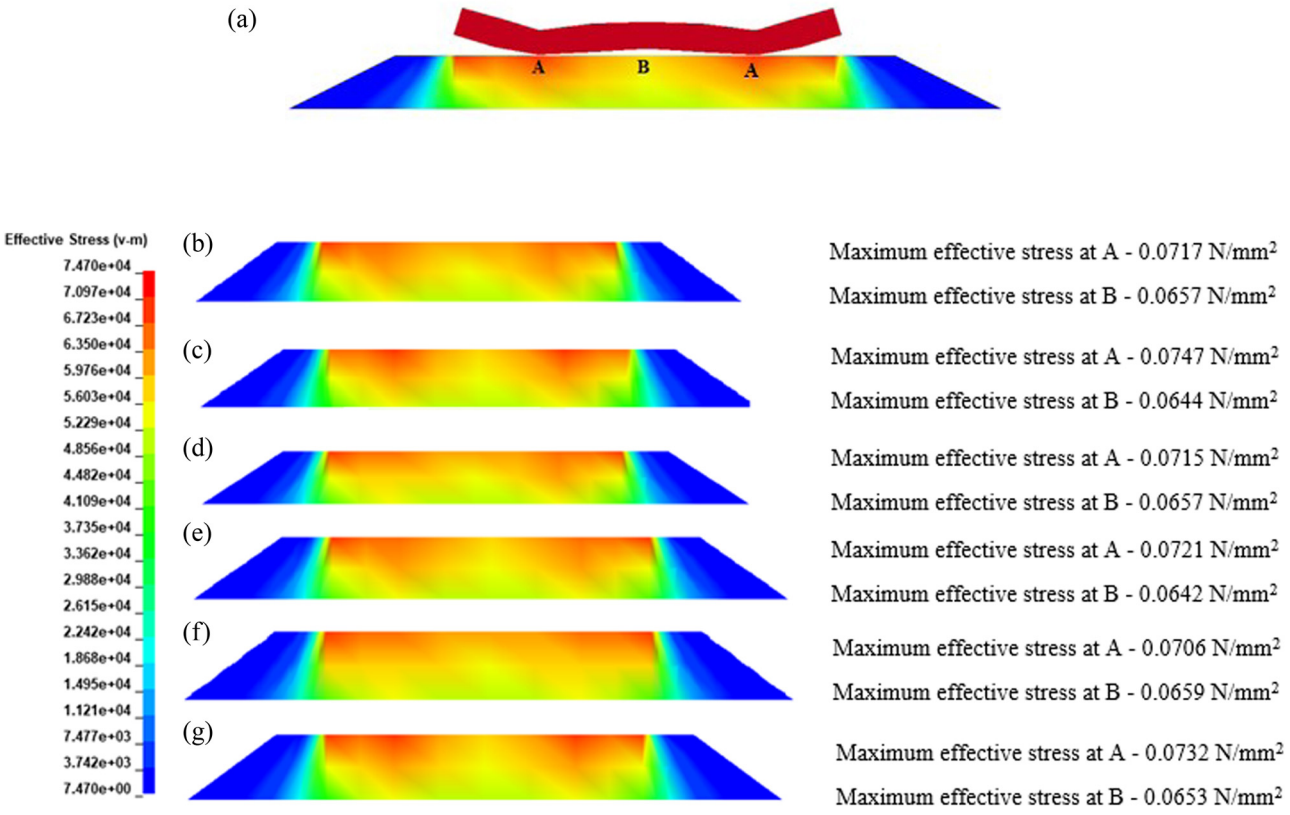

Figure 21: Effective stress distribution along ballast cross-section: (a) scaled image of deformation of sleeper and cross-section, (b) OCS, (c) RCS, (d) PFCS, (e) PFRS, (f) SFCS, (g) SFRS.

deformations of the sleeper. It is noted that the displacement at the rail seats is higher than that of the sleeper centre. As a result, the effective stress of higher magnitude can be noticed underneath the sleeper rail seats when compared to the ballast under the sleeper centre. The effective stress in ballast is the highest for RCS below the rail seats. The increase in effective stress in ballast under the sleeper is higher by 5 and 2%, respectively, when RCS and SFRS are tested on the tracks. About 1% decrease in effective stress in ballast under the sleeper can be noticed when SFCSs are used. Figure 20 illustrates the contour of effective stresses in ballast and presents the variation in stress contours for identical locations when different types of sleepers are adopted. The reduction of effective stresses at the sleeper centre can be observed when rubber concrete and fibre-reinforced RCSs are used. In comparison with the OCS and fibre-reinforced concrete sleepers, a significant reduction of stress intensities (change in contour intensity) is apparent. The variation is profoundly visible under the sleepers with critical mode shape which happens to be directly under a wheelset.

The effective stress distribution along the cross-section of the ballast is demonstrated in Figure 21. The w-shape bending of sleepers is presented in Figure 21(a). The rail seat and sleeper centre locations are marked as A and B, respectively, and peak stresses are noted in successive figures. The effective stress is higher underneath the rail seat locations of RCS and fibre-reinforced RCSs when compared to OCS and fibre-reinforced concrete sleepers. The aforementioned fact is highlighted by the lighter intensity of effective stress contours under the rail seats of OCS and fibre-reinforced concrete sleepers. It should also be mentioned that the intensity of stress contour under the sleeper centre is lighter for RCS and fibre-reinforced RCSs. The reason for the variation in stress contour can be explained with the help of Figure 21(a). It exhibits the scaled displacement of the sleepers placed over the ballast. The sleeper centre undergoes a slight uplift when compared to the rail seats owing to the peculiarity of the critical mode shape. When the wheels are placed over the rail seats, the sleeper centre experiences a hogging displacement pattern. However, from the perspective of overall displacement, the entire sleeper experiences downward displacement owing to the effect of the weight of the train. Hence, both the rail seats and the sleeper centre are subjected to some degree of effective stress. The hogging nature of displacement at

the sleeper centre helps to reduce the effective stresses. RCS are subjected to maximum rail seat displacement owing to the higher displacement for a given load. This higher rail seat displacement contributes to a higher hogging pattern at the sleeper centre. Hence, the effective stress under the sleeper centre is relatively minimal for RCS. Analogously, the minimum rail seat displacements in SFCS lead to minimum effective stresses underneath the rail seats of the sleeper and maximum effective stress under the sleeper centre. The results presented in this section will be limited to the track component properties given in Tables 6 and 7. The desirable stresses in ballast are limited to 0.3 N/mm^2 [82]. In the present case, the maximum effective stress in ballast is found to be less than 0.08 N/mm^2. It may also be noted that though the study was carried out based on the CRH 2 EMU, the RCSs and fibre-reinforced RCSs are suitable for trains with similar and lower axle loads.

4 Conclusions

In order to mitigate the damage caused to sleepers due to dynamic load, the study was carried out to enhance the impact resistance of sleepers using fibre-reinforced rubber concrete. The performance of ballasted tracks has been assessed for the novel applications of steel and PF-reinforced and pre-treated crumb RCSs by utilizing strain rate-dependent dynamic material properties. Engineering properties of ordinary concrete, pre-treated crumb rubber concrete, SF-reinforced concrete, SF-reinforced rubber concrete, PF-reinforced concrete, and PF-reinforced rubber concrete are demonstrated. A nonlinear numerical model for the ballasted tracks considering strain rate-dependent dynamic modulus of elasticity and yield stress of sleepers has been developed and fully validated by both experimental and numerical data. The sensitivity analyses have been rigorously carried out by varying the type of railway sleepers. The new insights derived from this study are drawn as follows:

- According to the modal analyses of railway sleepers under free–free conditions, the natural frequencies of railway sleepers will increase when SF is used. It can significantly improve the bending strength and toughness of the sleeper. However, adding rubber to a concrete sleeper tends to reduce the natural frequencies of the sleeper resulting in lesser bending stiffness despite having a lighter sleeper.
- The rail displacements increase with an increase in the train velocity. Maximum rail displacements can be observed when RCSs are adopted. The increase in rail displacement is 1.5% higher when RCSs are used.
- The rail seat sleeper displacements and sleeper centre displacement interestingly exhibit opposite trends. RCSs yield maximum rail seat displacements and minimum sleeper centre displacement. The magnitude of minimum rail seat displacement and maximum sleeper centre displacement is owned by SFCS. When RCS is used, a 5.5% increase in rail seat displacements is found in comparison with that obtained during the utilization of OCS. The rail seat displacements of SFRS are 2.5% higher than that of concrete sleepers. All the sleeper displacements are lower than the allowable limit of 5 mm prescribed for ballasted sleeper tracks.
- RCS, steel and PFRSs have lower amplitudes of acceleration and relatively higher damping when compared to their concrete counterparts. As a result, the increase in dynamic displacements of rail and sleepers is maintained at a relatively low percentage of about 5%.
- The effective stress in ballast is about 5% higher when an RCS is adopted compared to that of an OCS. Although the effective stress in the ballast under the rail seats of sleepers is the maximum for RCS, all the critical stresses are well within the desirable limits (0.3 N/mm^2).
- It is important to note that the adoption of every kilometre of RCS or fibre-reinforced RCSs helps the railway industry to save 16 tonnes of mineral aggregate and reduce up to 3.8 tonnes of crumb rubber, which is derived from domestic and industrial wastes.
- Analysis of the carbon footprint of rubber concrete and fibre-reinforced concrete sleepers reveals a reduction in embodied carbon for RCS and PFRS by 17.80 and 16.82%, respectively. However, a 19% increase in the magnitude of embodied carbon is observed for SFRS owing to the higher carbon footprint generated in the use of SFs compared to the carbon footprint of other constituent materials.

The new findings in our study reveal that all the sleepers considered, namely OCSs, pre-treated crumb RCSs, PFCSs, PFRSs, SFCSs, and SFRSs, perform well within permissible limits when considering the dynamic strain rate material model. The breakthrough discoveries provide new evidence and confidence about utilizing RCSs as well as steel and PFRSs in modern ballasted railway tracks. The application of fibre-reinforced rubber concrete will help the rail industry save about 16 tonnes of fine aggregates and decarbonize up to 3.8 tonnes of crumb rubber, thus proving the solutions as an eco-friendly and sustainable alternative to OCSs, thereby helping to preserve precious natural materials and by reducing the waste pile of worn-out tyre rubber. The RCSs and fibre-reinforced RCSs will have to be tested on a trial track in the field to assess their performance as part of future research.

Acknowledgments: The first author would like to express gratitude for the postdoctoral fellowship by the Second Century Fund (C2F), Chulalongkorn University.

Funding information: This Research is funded by the Thailand Science Research and Innovation Fund Chulalongkorn University (BCG66210020). This project is also funded by National Research Council of Thailand (NRCT). The authors also wish to acknowledge the Catalyst Grant funded by the Thai-UK World-class University Consortium, which is financially supported by the British Council and the Office of the Permanent Secretary, Ministry of Higher Education, Science, Research and Innovation. Financial support from the European Commission is acknowledged for H2020-MSCA-RISE (project no. 691135), which enables "Rail Infrastructure Systems Engineering Network (RISEN)" for global collaboration towards smart and resilient railway systems.

Author contributions: All authors have accepted responsibility for the entire content of this manuscript and approved its submission. AR: conceptualization, investigation, validation, formal analysis writing – original Draft. CN: conceptualization, validation, methodology, software, funding acquisition, project administration, writing – review and editing. LP: resources, investigation, writing – review and editing, supervision. SK: conceptualization, validation, funding acquisition, writing – review and editing, supervision.

Conflict of interest: The authors state no conflict of interest.

Data availability statement: All data generated or analysed during this study are included in this published article.

References

[1] Diziain D, Taniguchi E, Dablanc L. Urban logistics by rail and waterways in France and Japan. Procedia-Social Behav Sci. 2014 Mar;125:159–70.
[2] Cervero R, Murakami J. Rail and property development in Hong Kong: Experiences and extensions. Urban Stud. 2009 Sep;46(10):2019–43.
[3] Kaewunruen S, Remennikov AM. Effect of a large asymmetrical wheel burden on flexural response and failure of railway concrete sleepers in track systems. Eng Fail Anal. 2008 Dec;15(8):1065–75.
[4] Silva ÉA, Pokropski D, You R, Kaewunruen S. Comparison of structural design methods for railway composites and plastic sleepers and bearers. Aust J Struct Eng. 2017 Jul;18(3):160–77.
[5] Zakeri JA, Sadeghi J. Field investigation on load distribution and deflections of railway track sleepers. J Mech Sci Technol. 2007 Dec;21:1948–56.
[6] Iwnicki S. Handbook of railway vehicle dynamics. Boca Raton (FL), USA: CRC Press; 2006 May 22.
[7] Kaewunruen S, Remennikov AM. Impact capacity of railway prestressed concrete sleepers. Eng Fail Anal. 2009 Jul;16(5):1520–32.
[8] Ngamkhanong C, Kaewunruen S. Effects of under sleeper pads on dynamic responses of railway prestressed concrete sleepers subjected to high intensity impact loads. Eng Struct. 2020 Jul;214:110604.
[9] Zhai WM, Wang QC, Lu ZW, Wu XS. Dynamic effects of vehicles on tracks in the case of raising train speeds. Proc Inst Mech Eng Part F: J Rail and Rapid Transit. 2001 Mar;215(2):125–35.
[10] Kaewunruen S, Ngamkhanong C, Lim CH. Damage and failure modes of railway prestressed concrete sleepers with holes/web openings subject to impact loading conditions. Eng Struct. 2018 Dec;176:840–8.
[11] Ngamkhanong C, Li D, Remennikov AM, Kaewunruen S. Dynamic capacity reduction of railway prestressed concrete sleepers due to surface abrasions considering the effects of strain rate and prestressing losses. Int J Struct Stab Dyn. 2019 Jan;19(01):1940001.
[12] Bae HU, Yun KM, Moon J, Lim NH. Impact force evaluation of the derailment containment wall for high-speed train through a collision simulation. Adv Civ Eng. 2018;2018:1–4.
[13] Gupta T, Sharma RK, Chaudhary S. Impact resistance of concrete containing waste rubber fiber and silica fume. Int J Impact Eng. 2015 Sep 1;83:76–87.
[14] Topçu IB, Avcular N. Collision behaviours of rubberized concrete. Cem Concr Res. 1997 Dec;27(12):1893–8.
[15] He L, Cai H, Huang Y, Ma Y, Van Den Bergh W, Gaspar L, et al. Research on the properties of rubber concrete containing surface-modified rubber powders. J Build Eng. 2021 Mar;35:101991.
[16] Eldin NN, Senouci AB. Rubber-tire particles as concrete aggregate. J Mater Civ Eng. 1993 Nov;5(4):478–96.
[17] Medina NF, Medina DF, Hernández-Olivares F, Navacerrada MA. Mechanical and thermal properties of concrete incorporating rubber and fibres from tyre recycling. Constr Build Mater. 2017 Jul;144:563–73.
[18] Raj A, Nagarajan P, Aikot, Pallikkara S. Application of fiber-reinforced rubcrete in fencing posts. Pract Period Struct Des Constr. 2020 Nov;25(4):04020037.
[19] Murugan RB, Natarajan C, Chen SE. Material development for a sustainable precast concrete block pavement. J Traffic Transp Eng (Engl Ed). 2016 Oct;3(5):483–91.
[20] Feng W, Liu F, Yang F, Li L, Jing L. Experimental study on dynamic split tensile properties of rubber concrete. Constr Build Mater. 2018 Mar;165:675–87.
[21] Pham TM, Chen W, Khan AM, Hao H, Elchalakani M, Tran TM. Dynamic compressive properties of lightweight rubberized concrete. Constr Build Mater. 2020 Mar;238:117705.
[22] Liu F, Zheng W, Li L, Feng W, Ning G. Mechanical and fatigue performance of rubber concrete. Constr Build Mater. 2013 Oct;47:711–9.
[23] Zheng L, Huo XS, Yuan Y. Experimental investigation on dynamic properties of rubberized concrete. Constr Build Mater. 2008 May;22(5):939–47.
[24] Moustafa A, ElGawady MA. Mechanical properties of high strength concrete with scrap tire rubber. Constr Build Mater. 2015 Sep;93:249–56.
[25] Toutanji HA. The use of rubber tire particles in concrete to replace mineral aggregates. Cem Concr Compos. 1996 Jan;18(2):135–9.

[26] Li Z, Li F, Li JS. Properties of concrete incorporating rubber tyre particles. Mag Concr Res. 1998 Dec;50(4):297–304.
[27] Reda Taha MM, El-Dieb AS, Abd El-Wahab MA, Abdel-Hameed ME. Mechanical, fracture, and microstructural investigations of rubber concrete. J Mater Civ Eng. 2008 Oct;20(10):640–9.
[28] Atahan AO, Yücel AÖ. Crumb rubber in concrete: Static and dynamic evaluation. Constr Build Mater. 2012 Nov;36:617–22.
[29] Youssf O, Mills JE, Benn T, Zhuge Y, Ma X, Roychand R, et al. Development of crumb rubber concrete for practical application in the residential construction sector–design and processing. Constr Build Mater. 2020 Nov;260:119813.
[30] Jokar F, Khorram M, Karimi G, Hataf N. Experimental investigation of mechanical properties of crumbed rubber concrete containing natural zeolite. Constr Build Mater. 2019 May;208:651–8.
[31] Chou LH, Lu CK, Chang JR, Lee MT. Use of waste rubber as concrete additive. Waste Manag Res. 2007 Feb;25(1):68–76.
[32] Ganesan N, Raj B, Shashikala AP. Behavior of self-consolidating rubberized concrete beam-column joints. ACI Mater J. 2013 Nov;110(6):697.
[33] Barros JAO, Senacruz J. Fracture energy of steel fiber-reinforced concrete. Mech Compos Mater Struct. 2001;8:29–45.
[34] Nataraja MC, Dhang N, Gupta AP. Stress–strain curves for steel-fiber reinforced concrete under compression. Cem Concr Compos. 1999 Dec;21(5–6):383–90.
[35] Hao Y, Hao H. Dynamic compressive behaviour of spiral steel fibre reinforced concrete in split Hopkinson pressure bar tests. Constr Build Mater. 2013 Nov;48:521–32.
[36] Chen GM, He YH, Yang H, Chen JF, Guo YC. Compressive behavior of steel fiber reinforced recycled aggregate concrete after exposure to elevated temperatures. Constr Build Mater. 2014 Nov;71:1–5.
[37] Guo YC, Zhang JH, Chen GM, Xie ZH. Compressive behaviour of concrete structures incorporating recycled concrete aggregates, rubber crumb and reinforced with steel fibre, subjected to elevated temperatures. J Clean Prod. 2014 Jun;72:193–203.
[38] Şahin Y, Köksal F. The influences of matrix and steel fibre tensile strengths on the fracture energy of high-strength concrete. Constr Build Mater. 2011 Apr;25(4):1801–6.
[39] Yoo DY, Kim SW, Park JJ. Comparative flexural behavior of ultra-high-performance concrete reinforced with hybrid straight steel fibers. Constr Build Mater. 2017 Feb;132:219–29.
[40] Raj A, Nagarajan P, Shashikala AP. Application of fiber-reinforced rubcrete for crash barriers. J Mater Civ Eng. 2020 Dec;32(12):04020358.
[41] Xie JH, Guo YC, Liu LS, Xie ZH. Compressive and flexural behaviours of a new steel-fibre-reinforced recycled aggregate concrete with crumb rubber. Constr Build Mater. 2015 Mar;79:263–72.
[42] Yin S, Tuladhar R, Collister T, Combe M, Sivakugan N, Deng Z. Post-cracking performance of recycled polypropylene fibre in concrete. Constr Build Mater. 2015 Dec;101:1069–77.
[43] Bouziadi F, Boulekbache B, Hamrat M. The effects of fibres on the shrinkage of high-strength concrete under various curing temperatures. Constr Build Mater. 2016 Jul;114:40–8.
[44] Leong GW, Mo KH, Loh ZP, Ibrahim Z. Mechanical properties and drying shrinkage of lightweight cementitious composite incorporating perlite microspheres and polypropylene fibers. Constr Build Mater. 2020;245:118410. doi: 10.1016/j.conbuildmat.2020.118410.
[45] Song PS, Hwang S, Sheu BC. Strength properties of nylon-and polypropylene-fiber-reinforced concretes. Cem Concr Res. 2005 Aug;35(8):1546–50.
[46] Libre NA, Shekarchi M, Mahoutian M, Soroushian P. Mechanical properties of hybrid fiber reinforced lightweight aggregate concrete made with natural pumice. Constr Build Mater. 2011 May;25(5):2458–64.
[47] Raj A, Usman Arshad PJ, Nagarajan P, Shashikala AP. Experimental investigation on the fracture behaviour of polypropylene fibre-reinforced rubcrete. In: Prakash R, Suresh Kumar R, Nagesha A, Sasikala G, Bhaduri A, editors. Structural Integrity Assesment. Lecture Notes in Mechanical Engineering. Singapore: Springer. p. 335–45.
[48] Alsaif A, Koutas L, Bernal SA, Guadagnini M, Pilakoutas K. Mechanical performance of steel fibre reinforced rubberised concrete for flexible concrete pavements. Constr Build Mater. 2018 May;172:533–43.
[49] Noaman AT, Bakar BA, Akil HM, Alani AH. Fracture characteristics of plain and steel fibre reinforced rubberized concrete. Constr Build Mater. 2017 Oct;152:414–23.
[50] Noaman AT, Bakar BA, Akil HM. Experimental investigation on compression toughness of rubberized steel fibre concrete. Constr Build Mater. 2016 Jul;115:163–70.
[51] Ganesan N, Indira PV, Sabeena MV. Behaviour of hybrid fibre reinforced concrete beam–column joints under reverse cyclic loads. Mater Des (1980-2015). 2014 Feb;54:686–93.
[52] Soufeiani L, Raman SN, Jumaat MZ, Alengaram UJ, Ghadyani G, Mendis P. Influences of the volume fraction and shape of steel fibers on fiber-reinforced concrete subjected to dynamic loading–A review. Eng Struct. 2016 Oct;124:405–17.
[53] Kaewunruen S, Li D, Chen Y, Xiang Z. Enhancement of dynamic damping in eco-friendly railway concrete sleepers using waste-tyre crumb rubber. Materials. 2018 Jul;11(7):1169.
[54] Parvez A, Foster SJ. Fatigue of steel-fibre-reinforced concrete prestressed railway sleepers. Eng Struct. 2017 Jun;141:241–50.
[55] Shakeri A, Remennikov AM, Sheikh MN. Development of fibre-reinforced concrete mix for manufacturing non-prestressed concrete sleepers. Structures. 2022;37:588–99.
[56] Yoo DY, Lee JY, Shin HO, Yang JM, Yoon YS. Effects of blast furnace slag and steel fiber on the impact resistance of railway prestressed concrete sleepers. Cem Concr Compos. 2019 May;99:151–64.
[57] Ramezanianpour AA, Esmaeili M, Ghahari SA, Najafi MH. Laboratory study on the effect of polypropylene fiber on durability, and physical and mechanical characteristic of concrete for application in sleepers. Constr Build Mater. 2013 Jul;44:411–8.
[58] Jing G, Yunchang D, You R, Siahkouhi M. Comparison study of crack propagation in rubberized and conventional prestressed concrete sleepers using digital image correlation. Proc Inst Mech Eng Part F: J Rail Rapid Transit. 2022 Apr;236(4):350–61.
[59] Raj A, Nagarajan P, Shashikala AP. Investigations on fiber-reinforced rubcrete for railway sleepers. ACI Struct J. 2020 Sep;117(5):109–20.
[60] Klasztorny M, Szurgott P. Modeling and simulation of bridge–track–train systems at high service velocities with LS-DYNA®. In: Oswald R, editor. 12th International LS-DYNA Users Conference; 2012 Jun 3–5; Dearborn (MI), USA. Livermore Software Technology Corporation, 2012.
[61] Abebe MS, Qiu HS. Numerical modeling of geotextile reinforcement of soft subgrade ballasted railway under high speed train. Electron J Geotech Eng. 2016;21(12):4327–43.
[62] Ngamkhanong C, Ming QY, Li T, Kaewunruen S. Dynamic train-track interactions over railway track stiffness transition zones using baseplate fastening systems. Eng Fail Anal. 2020 Dec;118:104866.

[63] Costa PA, Calçada R, Cardoso AS. Ballast mats for the reduction of railway traffic vibrations. Numerical study. Soil Dyn Earthq Eng. 2012 Nov;42:137–50.
[64] Costa PA, Calçada R, Cardoso AS. Track–ground vibrations induced by railway traffic: In-situ measurements and validation of a 2.5 D FEM-BEM model. Soil Dyn Earthq Eng. 2012 Jan;32(1):111–28.
[65] Li T, Su Q, Kaewunruen S. Influences of dynamic material properties of slab track components on the train-track vibration interactions. Eng Fail Anal. 2020 Sep;115:104633.
[66] Habib A, Yildirim U, Eren O. Mechanical and dynamic properties of high strength concrete with well graded coarse and fine tire rubber. Constr Build Mater. 2020 Jun;246:118502.
[67] Najim KB, Hall MR. Mechanical and dynamic properties of self-compacting crumb rubber modified concrete. Constr Build Mater. 2012 Feb;27(1):521–30.
[68] Hameed AS, Shashikala AP. Suitability of rubber concrete for railway sleepers. Perspect Sci. 2016 Sep;8:32–5.
[69] Long WJ, Li HD, Wei JJ, Xing F, Han N. Sustainable use of recycled crumb rubbers in eco-friendly alkali activated slag mortar: Dynamic mechanical properties. J Clean Prod. 2018 Dec;204:1004–15.
[70] Yu J, Chen Y, Leung CK. Mechanical performance of Strain-Hardening Cementitious Composites (SHCC) with hybrid polyvinyl alcohol and steel fibers. Compos Struct. 2019 Oct;226:111198.
[71] Kumar R, Shafiq N, Kumar A, Jhatial AA. Investigating embodied carbon, mechanical properties, and durability of high-performance concrete using ternary and quaternary blends of metakaolin, nano-silica, and fly ash. Environ Sci Pollut Res. 2021 Sep;28:49074–88.
[72] Chen M, Zhong H, Chen L, Zhang Y, Zhang M. Engineering properties and sustainability assessment of recycled fibre reinforced rubberised cementitious composite. J Clean Prod. 2021 Jan 1;278:123996.
[73] IS 383. Coarse and fine aggregate for concrete–specification. Bureau of Indian Standards. 2016 Jan.
[74] ACI 544.2R-11. Measurement of properties of fiber-reinforced concrete. 1996.
[75] IS 516. Method of tests for strength of concrete. Bureau of Indian Standards. 1959 Dec.
[76] IS 13030. Method of test for laboratory determination of water content, porosity, density and related properties of rock material. Bureau of Indian Standards. 1991 May.
[77] Schwer L. The Winfrith concrete model: Beauty or beast? Insights into the Winfrith concrete model. In: 8th European LS-DYNA Users Conference; 2011 May 23–24; Strasbourg, France. DynaMORE, 2011.
[78] Jiang H, Chorzepa MG. An effective numerical simulation methodology to predict the impact response of pre-stressed concrete members. Eng Fail Anal. 2015 Sep;55:63–78.
[79] CEB. Plenary Session. Concrete structures under impact and impulsive loading: Synthesis report. Lausanne, Switzerland: Comite Euro-International du Beton; 1988.
[80] Zhang X, Zhao C, Zhai W. Dynamic behavior analysis of high-speed railway ballast under moving vehicle loads using discrete element method. Int J Geomech. 2017 Jul;17(7):04016157.
[81] Chinese Standard: TB 10761-2013. Technical regulations for dynamic acceptance for high-speed railways construction. TB. 2013;10761–2013.
[82] Sañudo R, Miranda M, Alonso B, Markine V. Sleepers spacing analysis in railway track infrastructure. Infrastructures. 2022 Jun;7(6):83.
[83] Salih C, Manalo A, Ferdous W, Yu P, Abousnina R, Heyer T, et al. Effect of bending and compressive modulus of elasticity on the behaviour of timber-alternative railway sleepers supported by ballast. Case Stud Constr Mater. 2021 Dec;15:e00597.